Cytoplasmic γ-actin and tropomodulin isoforms link to the sarcoplasmic reticulum in skeletal muscle fibers

David S. Gokhin and Velia M. Fowler

Department of Cell Biology, The Scripps Research Institute, La Jolla, CA 92037

The sarcoplasmic reticulum (SR) serves as the Ca^{2+} reservoir for muscle contraction. Tropomodulins (Tmods) cap filamentous actin (F-actin) pointed ends, bind tropomyosins (Tms), and regulate F-actin organization. In this paper, we use a genetic targeting approach to examine the effect of Tmod1 deletion on the organization of cytoplasmic γ-actin (γ_{cyto}-actin) in the SR of skeletal muscle. In wild-type muscle fibers, γ_{cyto}-actin and Tmod3 defined an SR microdomain that was distinct from another Z line–flanking SR microdomain containing Tmod1 and Tmod4. The γ_{cyto}-actin/Tmod3 microdomain contained an M line complex composed of small ankyrin 1.5 (sAnk1.5), γ_{cyto}-actin, Tmod3, Tm4, and Tm5NM1. Tmod1 deletion caused Tmod3 to leave its SR compartment, leading to mislocalization and destabilization of the Tmod3–γ_{cyto}-actin–sAnk1.5 complex. This was accompanied by SR morphological defects, impaired Ca^{2+} release, and an age-dependent increase in sarcomere misalignment. Thus, Tmod3 regulates SR-associated γ_{cyto}-actin architecture, mechanically stabilizes the SR via a novel cytoskeletal linkage to sAnk1.5, and maintains the alignment of adjacent myofibrils.

Introduction

Striated muscle contraction is built on an exquisitely regulated actin cytoskeleton, where actin isoforms sort into distinct, non-overlapping compartments. The thin filaments of sarcomeres consist of skeletal muscle α-actin (α_{sk}-actin), whereas extrasarcomeric membrane compartments contain cytoplasmic γ-actin (γ_{cyto}-actin; Craig and Pardo, 1983; Pardo et al., 1983; Otey et al., 1988; Rybakova et al., 2000). The lengths of α_{sk}-actin thin filaments are determined by α_{sk}-actin monomer exchange at pointed ends, which is in turn regulated by tropomodulins (Tmods), a family of tropomyosin (Tm)-binding and pointed end–capping proteins (Gregorio et al., 1995; Littlefield et al., 2001; Littlefield and Fowler, 2008). In contrast, it is unknown whether Tmods regulate the lengths, stability, and/or organization of γ_{cyto}-actin filaments, which are proposed to fortify the sarcolemma through their interactions with dystrophin and β2-spectrin at costameres (Craig and Pardo, 1983; Porter et al., 1992, 1997; Renley et al., 1998; Rybakova et al., 2000;

Williams et al., 2001). γ_{cyto}-Actin is dispensable for skeletal muscle development, but its absence can produce muscle weakness, indicating that γ_{cyto}-actin plays a role in muscle mechanical performance (Sonnemann et al., 2006; Belyantseva et al., 2009). Surprisingly, γ_{cyto}-actin–deficient muscles do not exhibit sarcolemmal defects, leaving the functional role of γ_{cyto}-actin in muscle membranes uncertain (Sonnemann et al., 2006). However, up to 10-fold up-regulation of γ_{cyto}-actin has been observed in various animal models of muscular dystrophy, including dystrophin-deficient *mdx* mice, α-sarcoglycan–null mice, and golden retriever muscular dystrophy (Hanft et al., 2006, 2007). Thus, the importance of γ_{cyto}-actin under pathological conditions suggests possible functions for γ_{cyto}-actin in the structural biology of other striated muscle membranes such as the sarcoplasmic reticulum (SR).

Four Tmod isoforms could potentially regulate extrasarcomeric γ_{cyto}-actin organization in skeletal muscle. Tmod1 is found predominantly in terminally differentiated postmitotic cells (such as erythrocytes, lens fiber cells, neurons, and striated muscle),

The Rockefeller University Press $30.00
J. Cell Biol. Vol. 194 No. 1   105–120
www.jcb.org/cgi/doi/10.1083/jcb.201011128

JCB   **105**

Tmod2 is predominantly in neuronal tissues, Tmod3 is ubiquitous, and Tmod4 is restricted to skeletal muscle fibers (Fowler, 1987, 1990; Sung et al., 1992; Watakabe et al., 1996; Almenar-Queralt et al., 1999; Cox and Zoghbi, 2000; Conley et al., 2001). Of these isoforms, only Tmod1 and Tmod4 normally localize to thin filament pointed ends in skeletal muscle (Fowler et al., 1993; Almenar-Queralt et al., 1999; Gokhin et al., 2010). However, Tmod1 also colocalizes with α2-spectrin at the sarcolemma of fast muscle fibers in the chicken (Almenar-Queralt et al., 1999) and can be detected at the A band/I band junction in isolated rat skeletal myofibrils (Fowler et al., 1993). Furthermore, Tmod3 localizes to the M line and regions flanking the Z line in mouse muscles (Gokhin et al., 2010), which recapitulates the localizations of nonmuscle Tm4 and Tm5NM1 in the SR and intracellular membranes (Kee et al., 2004; Vlahovich et al., 2008, 2009). Therefore, based on their localizations at structures other than thin filament pointed ends, Tmods are likely candidates for capping extrasarcomeric γ_{cyto}-actin and determining γ_{cyto}-actin architecture in skeletal muscle. Because Tmod1 is known to regulate the architecture of nonmuscle F-actin in the spectrin-based membrane skeletons of nonmuscle cells (Nowak et al., 2009; Moyer et al., 2010), we hypothesized that perturbation of Tmod1 expression might alter extrasarcomeric γ_{cyto}-actin architecture and provide clues about the function of γ_{cyto}-actin in skeletal muscle.

To address our hypothesis, we used a genetic targeting approach to delete Tmod1 from skeletal muscle. Tmod1-null mice are embryonic lethal at embryonic day (E) 9.5 (Chu et al., 2003; Fritz-Six et al., 2003), but we were able to rescue their lethality with a cardiac-specific transgene that places Tmod1 under the control of the α–myosin heavy chain (α-MHC) promoter ($Tmod1^{-/-Tg(\alpha-MHC–Tmod1)}$, hereafter referred to as $Tmod1^{-/-Tg+}$; McKeown et al., 2008). This enabled us to study the role of Tmod1 in skeletal muscle fibers, which start to develop at about E13 in the mouse (Miller, 1991). $Tmod1^{-/-Tg+}$ muscle generates less isometric stress than $Tmod1^{+/+Tg+}$ muscle, but this cannot be explained by changes in thin filament length in the absence of Tmod1, as compensatory substitution by Tmod3 and Tmod4 at thin filament pointed ends functions to maintain correct thin filament lengths (Gokhin et al., 2010). This led us to speculate that the weakness of $Tmod1^{-/-Tg+}$ skeletal muscle may be a result of additional deficits arising from abnormalities in the extrasarcomeric actin cytoskeleton. In this study, we show that Tmod3 and γ_{cyto}-actin establish an SR microdomain that is distinct from a second microdomain containing Tmod1 and Tmod4. The γ_{cyto}-actin/Tmod3 microdomain is associated with an M line complex also containing small ankyrin 1.5 (sAnk1.5) and nonmuscle Tm4 and Tm5NM1. Deletion of Tmod1 causes Tmod3 to vacate its M line SR compartment and translocate to the thin filament pointed ends, leading to altered localization of sAnk1.5, γ_{cyto}-actin, Tm4, and Tm5NM1, abnormal SR morphologies, defects in Ca^{2+} handling, and an increase in sarcomere misalignment that is more pronounced in more heavily recruited muscles. Deletion of Tmod1 does not affect the organization of the β2-spectrin–ankyrin-B membrane skeleton, the desmin intermediate filament system, or the dystrophin–glycoprotein complex (DGC). We propose that Tmod3 mediates the organization of γ_{cyto}-actin via binding to sAnk1.5, thereby providing SR stabilization, extrasarcomeric cytoskeletal connectivity, and a novel cytoskeletal linkage that facilitates lateral force transmission across muscle fibers.

Results

A cytoskeleton containing γ_{cyto}-actin, Tmods, and spectrin localizes to extrasarcomeric compartments in skeletal muscle

We defined the architecture of γ_{cyto}-actin in wild-type skeletal muscle by immunostaining transverse cryosections of tibialis anterior (TA) and soleus muscles from 1-mo-old mice for γ_{cyto}-actin and its binding partner β2-spectrin (Fig. 1 A). Capillaries dominated the γ_{cyto}-actin staining at the fiber bundle level and provided an internal positive control for γ_{cyto}-actin immunoreactivity, as expected from the abundance of γ_{cyto}-actin in endothelial cells (Galustian et al., 1995). However, a punctate γ_{cyto}-actin staining pattern was still evident within the muscle fibers. Upon higher magnification examination of single fibers, γ_{cyto}-actin exhibited partial colocalization with β2-spectrin at the sarcolemma, as expected (Repasky et al., 1982; Craig and Pardo, 1983; Nelson and Lazarides, 1983). Importantly, γ_{cyto}-actin did not colocalize at all with the myofibrils, which were identified by phalloidin staining for F-actin, confirming that the antibodies to γ_{cyto}-actin did not cross react with α_{sk}-actin in myofibrils. We observed instead that γ_{cyto}-actin and β2-spectrin localized to the intermyofibrillar compartments, which contain vesicular and membrane systems, mitochondria, and cytoplasmic components in skeletal muscle, consistent with previous observations that spectrin forms a reticular network between myofibrils (Repasky et al., 1982; Craig and Pardo, 1983). Identical γ_{cyto}-actin staining patterns were observed using both rabbit pAb 7577 (Fig. 1 A; Hanft et al., 2006) and mouse mAb A8481 (Fig. 1, B and C), whose specificities were established using Western blotting on cell and tissue lysates with known actin isoform inventories (Fig. S1). Phalloidin stained myofibrillar α_{sk}-actin but not the compartments containing γ_{cyto}-actin (Fig. 1), even though phalloidin binds F-actin regardless of its actin isoform composition (Allen et al., 1996). We attribute this to the ∼4,500-fold greater abundance of α_{sk}-actin in myofibrils compared with γ_{cyto}-actin in skeletal muscle (Hanft et al., 2006), which thus predominates over the γ_{cyto}-actin signal.

Both Tmod1 and Tmod3 have been shown to associate with extrasarcomeric structures (Almenar-Queralt et al., 1999; Gokhin et al., 2010). To determine the localizations of these Tmods with respect to extrasarcomeric γ_{cyto}-actin, we immunostained transverse sections of TA and soleus muscle for γ_{cyto}-actin and either Tmod1 or Tmod3. Both Tmod1 and Tmod3 colocalized with γ_{cyto}-actin in extrasarcomeric compartments in wild-type muscle (Fig. 1, B and C), indicating that a combination of at least Tmod1 and Tmod3 can cap γ_{cyto}-actin filament pointed ends in normal skeletal muscle. Capillaries exhibited the most pronounced Tmod3 fluorescence and provided an internal positive control for Tmod3 immunoreactivity, as Tmod3 is the unique Tmod isoform in the endothelial cells that comprise the microvasculature (Fischer et al., 2003).
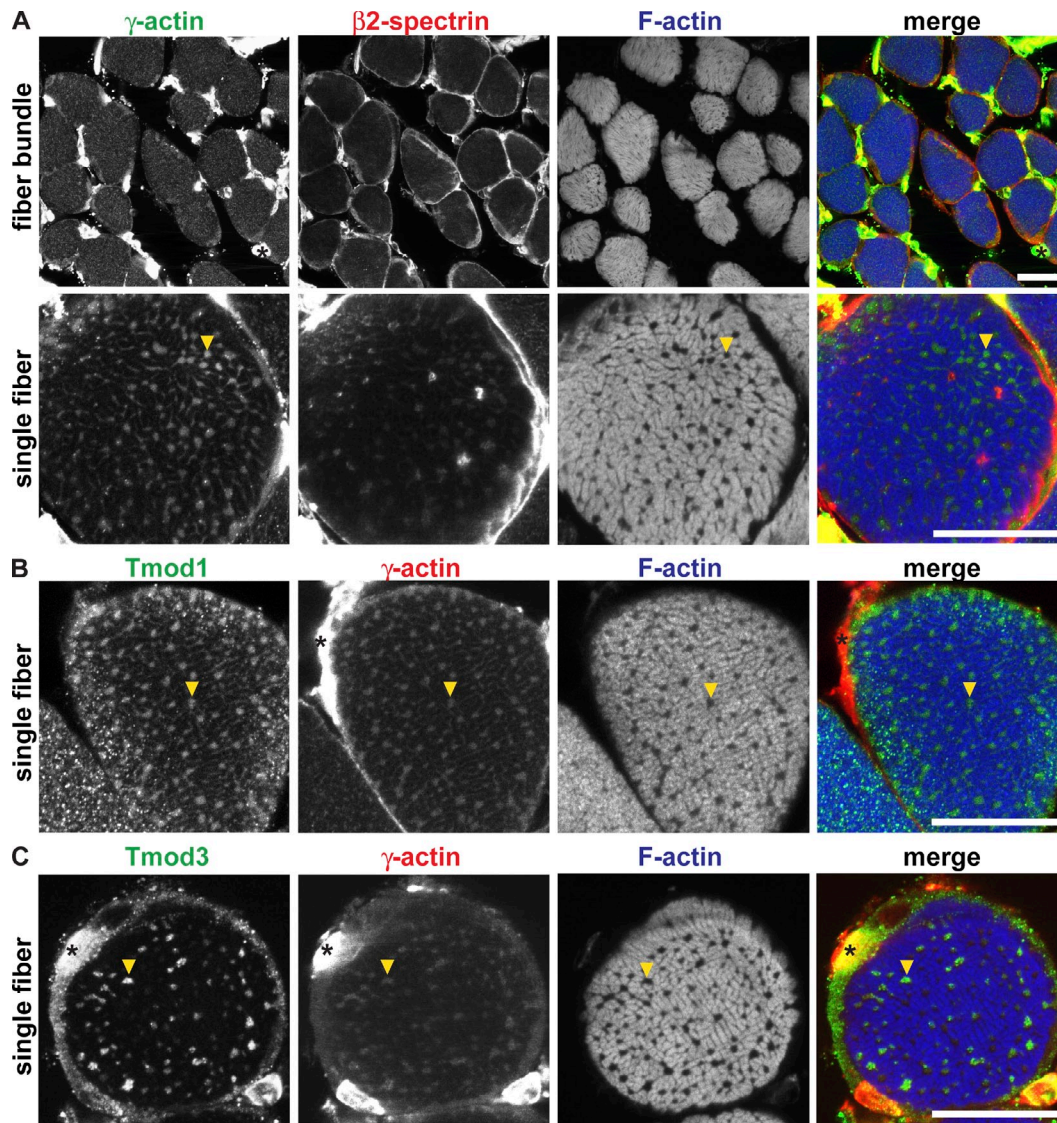
Figure 1. **Tmods, γ_{cyto}-actin, and spectrin localize to intermyofibrillar compartments in skeletal muscle.** (A–C) Transverse cryosections of 1-mo-old TA muscle fiber bundles and single fibers immunostained for γ_{cyto}-actin, β2-spectrin, and F-actin (A) or γ_{cyto}-actin, F-actin, and either Tmod1 (B) or Tmod3 (C). Arrowheads indicate intermyofibrillar compartments enriched for Tmods, γ_{cyto}-actin, and β2-spectrin. Asterisks indicate capillaries. Bars, 25 µm.

Deletion of Tmod1 perturbs the extrasarcomeric γ_{cyto}-actin cytoskeleton

To investigate a potential role for Tmod1 in organizing γ_{cyto}-actin with respect to myofibril/sarcomere striations, we immunostained longitudinal sections of $Tmod1^{-/-Tg+}$ and $Tmod1^{+/+Tg+}$ TA muscle for γ_{cyto}-actin and Tmods. In $Tmod1^{+/+Tg+}$ muscle, Tmod1 and Tmod4 exhibited their well-established localization at the pointed ends of phalloidin-stained thin filaments, but these Tmods also localized to fainter stripes flanking the Z line (Figs. 2 A and S2). Tmod1 fluorescence was not detectable in $Tmod1^{-/-Tg+}$ muscle (Fig. 2 A), as expected (Gokhin et al., 2010). Tmod3 localized to the M line and to a wide stripe overlying the Z line in $Tmod1^{+/+Tg+}$ muscle, redistributing to thin filament pointed ends in $Tmod1^{-/-Tg+}$ muscle (Fig. 2 B), as shown previously (Gokhin et al., 2010). Notably, γ_{cyto}-actin colocalized with Tmod3 at the M line and in a wide Z line–flanking stripe in $Tmod1^{+/+Tg+}$ muscle (Fig. 2 B). Furthermore,

γ_{cyto}-actin partially colocalized with the narrow Z line–flanking Tmod1 doublets in $Tmod1^{+/+Tg+}$ muscle and the Z line–flanking Tmod4 doublets in both $Tmod1^{+/+Tg+}$ and $Tmod1^{-/-Tg+}$ muscle (Figs. 2 A and S2). Examination of highly stretched myofibrils did not reveal any M line–associated Tmod1 or Tmod4 that might have been obscured by the bright Tmod1 or Tmod4 fluorescence at thin filament pointed ends (unpublished data). Thus, Tmod3 and γ_{cyto}-actin define an extrasarcomeric compartment whose signature is an M line stripe and a wide Z line stripe, whereas Tmod1 and Tmod4 are predominantly associated with thin filament pointed ends, with a minor component localized to a second extrasarcomeric compartment whose signature is a doublet of narrow Z line–flanking stripes.

Although γ_{cyto}-actin localized to the M line and across the Z line in both $Tmod1^{+/+Tg+}$ and $Tmod1^{-/-Tg+}$ muscle, we noticed a modest attenuation of M line γ_{cyto}-actin fluorescence in $Tmod1^{-/-Tg+}$ muscle (Fig. 2, A–C). To quantify this change,
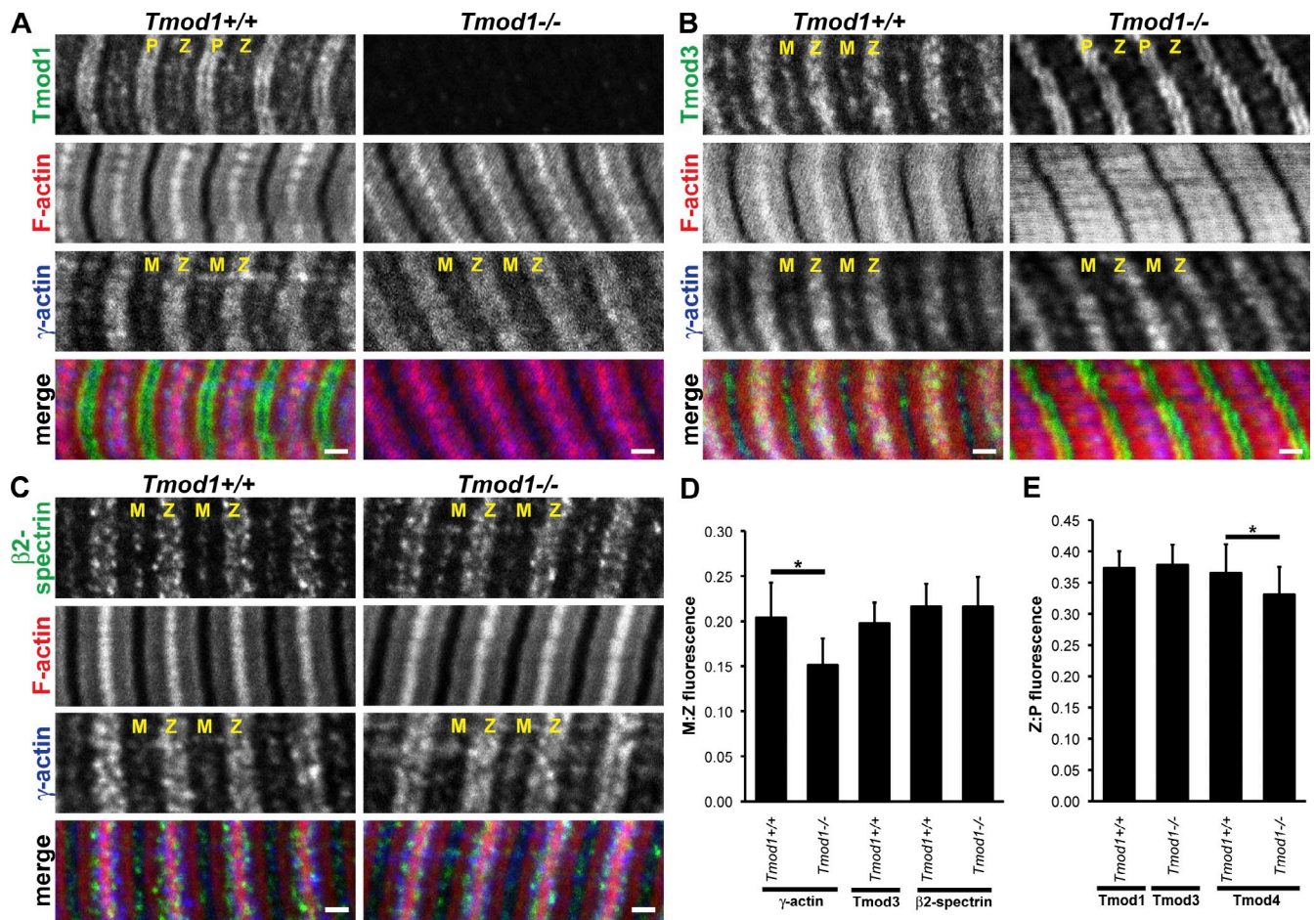
Figure 2. **Tmods and γ_cyto-actin exhibit two distinct extrasarcomeric localizations at the M line and flanking the Z line, and deletion of Tmod1 depletes γ_cyto-actin from the M line.** (A–C) Longitudinal cryosections of 1-mo-old TA muscle fibers from *Tmod1*⁺/⁺ᵀᵍ⁺ and *Tmod1*⁻/⁻ᵀᵍ⁺ mice immunostained for γ_cyto-actin, F-actin, and either Tmod1 (A), Tmod3 (B), or β2-spectrin (C). (D and E) Quantitation of the ratio of M/Z (D) and Z/P (E) fluorescence of γ_cyto-actin, β2-spectrin, and Tmods. Each bar reflects n = 91–99 myofibrils/genotype measured from three mice (six muscles)/genotype for γ_cyto-actin, β2-spectrin, and Tmod3 or n = 42–83 myofibrils/genotype measured from two mice (four muscles)/genotype for Tmod1 and Tmod4. *, P < 0.001. M, M line; P, thin filament pointed ends; Z, Z line. Data are presented as mean ± SD. Bars, 1 µm.

we integrated γ_cyto-actin fluorescence intensity along line scans of myofibrils and measured the ratio of M line to Z line (M/Z) fluorescence. We found that the ratio of M/Z fluorescence decreased from ∼0.20 in *Tmod1*⁺/⁺ᵀᵍ⁺ muscle to ∼0.15 in *Tmod1*⁻/⁻ᵀᵍ⁺ muscle, a decrease of ∼25% (Fig. 2 D), which suggests that the deletion of Tmod1 and concomitant translocation of Tmod3 alter the architecture of extrasarcomeric γ_cyto-actin in skeletal muscle. However, the total levels of γ_cyto-actin were unchanged in *Tmod1*⁻/⁻ᵀᵍ⁺ muscle (Fig. S3), similar to Tmod3 (Gokhin et al., 2010). Interestingly, the ratio of Tmod3 M/Z fluorescence in *Tmod1*⁺/⁺ᵀᵍ⁺ muscle was also ∼0.20 (Fig. 2 D), indicating that γ_cyto-actin and Tmod3 are partitioned with a similar pattern across extrasarcomeric striated compartments. Thus, γ_cyto-actin is associated with Tmod3 in an extrasarcomeric cytoskeletal compartment overlaying the M line and in a broad band flanking the Z line.

A similar quantitative image analysis was performed for the ratio of Z line to pointed end (Z/P) fluorescence for Tmod1 in *Tmod1*⁺/⁺ᵀᵍ⁺ muscle, Tmod3 in *Tmod1*⁻/⁻ᵀᵍ⁺ muscle, and Tmod4 in both *Tmod1*⁺/⁺ᵀᵍ⁺ and *Tmod1*⁻/⁻ᵀᵍ⁺ muscle. The ratio of Z/P fluorescence was ∼0.37 for all Tmods, although a modest but

statistically significant decrease in Tmod4 Z/P fluorescence was observed in *Tmod1*⁻/⁻ᵀᵍ⁺ muscle (Fig. 2 E). This suggests that a small amount of Tmod4 is lost from the Z line–flanking doublets, redistributing to the thin filament pointed ends in the absence of Tmod1. These observations strengthen the notion that both Tmod3 and Tmod4 structurally compensate for the absence of Tmod1 by capping thin filament pointed ends (Gokhin et al., 2010).

To determine whether γ_cyto-actin and Tmod3 at the M line and spanning across the Z line were associated with a spectrin cytoskeleton, we immunostained longitudinal sections of TA muscle for γ_cyto-actin and β2-spectrin. Both γ_cyto-actin and β2-spectrin localized in a narrow band at the M line and in a broad band across the Z line in both *Tmod1*⁺/⁺ᵀᵍ⁺ and *Tmod1*⁻/⁻ᵀᵍ⁺ muscle (Fig. 2 C). In contrast to γ_cyto-actin, the ratio of β2-spectrin M/Z fluorescence was unchanged in *Tmod1*⁻/⁻ᵀᵍ⁺ muscle (Fig. 2 D). Western blotting also showed no changes in β2-spectrin levels in *Tmod1*⁻/⁻ᵀᵍ⁺ muscle (Fig. S3). Thus, β2-spectrin shares an extrasarcomeric compartment with γ_cyto-actin and Tmod3, but γ_cyto-actin alterations and Tmod3 translocation downstream of Tmod1 deletion do not perturb the extrasarcomeric spectrin network.

Tmods and γ_{cyto}-actin define two distinct SR microdomains

The SR membrane system wraps around myofibrils and serves as the Ca²⁺ reservoir for muscle contraction. The SR membranes flank the Z line, where the terminal cisternae of the longitudinal SR are coupled to the transverse tubules at the triads, and are also located at the M line, where the fenestrated collar forms a sheath around the center of the sarcomere. Immunostaining of longitudinal sections of $Tmod1^{+/+Tg+}$ and $Tmod1^{-/-Tg+}$ muscle revealed that two key SR-associated Ca²⁺ channels in skeletal muscle, RyR1 and sarco/ER Ca²⁺ ATPase 1 (SERCA1), localize in a striated pattern at the M line and flanking the Z line. In both $Tmod1^{+/+Tg+}$ and $Tmod1^{-/-Tg+}$ muscle, RyR1 staining was predominantly enriched at the M line with fainter Z line–flanking stripes in a pattern distinct from either Tmods or γ_{cyto}-actin (Fig. 3 A), whereas SERCA1 staining was present in a broad band around the Z line with a fainter M line stripe, resembling the staining patterns of γ_{cyto}-actin, Tmod3, and β2-spectrin (Fig. 3 B). For both RyR1 and SERCA1, total protein levels and the ratio of M/Z fluorescence were identical in $Tmod1^{+/+Tg+}$ and $Tmod1^{-/-Tg+}$ muscle (unpublished data). These data suggest that extrasarcomeric γ_{cyto}-actin, Tmod3, and β2-spectrin are associated with an SR compartment also containing SERCA1, whereas Tmod1 and Tmod4 may be associated with a subdomain of the RyR1-containing SR compartment flanking the Z line. However, Tmod1 deletion affects neither the levels nor the localization of these two major SR-associated Ca²⁺ channels.

To discern in more detail how actins and Tmods sort across skeletal muscle compartments, we subjected $Tmod1^{+/+Tg+}$ and $Tmod1^{-/-Tg+}$ TA muscle homogenates to differential centrifugation and Western blotting for α_{sk}-actin, RyR1, SERCA1, γ_{cyto}-actin, Tmod1, Tmod3, and Tmod4 (Fig. 4). As expected from previous differential centrifugation experiments (Knight and Trinick, 1982; Fowler et al., 1993), ∼90% of α_{sk}-actin was contained in the 1,500-g pellet (which mainly contains myofibrils), and the remaining 10% was in the cytosol. Both RyR1 and SERCA were predominantly in the 15,000-g pellet (which mainly contains membranes and organelles) and the 150,000-g pellet (which mainly contains microsomes and macromolecular complexes) of muscles of both genotypes. Although γ_{cyto}-actin and Tmod3 were present in all fractions, they were enriched in the 15,000- and 150,000-g pellets, tending to cofractionate with the SR markers. Tmod1 and Tmod4 fractionated predominantly in the 1,500-g pellet along with the myofibrils, with smaller fractions in the 15,000-g pellet and cytosol. Thus, Tmod1 and Tmod4 have a biochemical fractionation signature distinct from γ_{cyto}-actin and Tmod3, consistent with the distinct immunofluorescence staining signatures of Tmod1/Tmod4 versus γ_{cyto}-actin/Tmod3 (Fig. 2). The fraction of Tmod3 in the 1,500-g myofibrillar pellet increased from ∼17% in $Tmod1^{+/+Tg+}$ muscle to ∼33% in $Tmod1^{-/-Tg+}$ muscle and was accompanied by a corresponding depletion of Tmod3 from the cytosol fraction, consistent with Tmod3 translocation to thin filament pointed ends in the absence of Tmod1 (Fig. 2 B; Gokhin et al., 2010). The fraction of Tmod4 in the 1,500-g pellet increased from ∼46% in $Tmod1^{+/+Tg+}$ muscle to ∼53% in $Tmod1^{-/-Tg+}$ muscle, again consistent with a small amount of Tmod4 translocation to
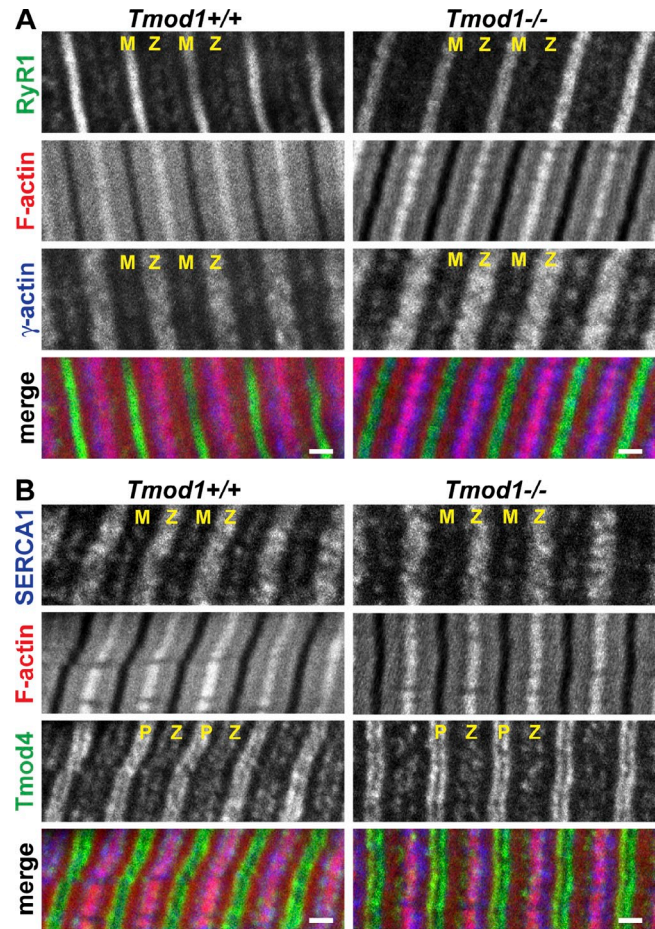

Figure 3. **Extrasarcomeric structures containing γ_{cyto}-actin and Tmods co-localize with the SR.** (A and B) Longitudinal cryosections of 1-mo-old TA muscle fibers from $Tmod1^{+/+Tg+}$ and $Tmod1^{-/-Tg+}$ mice immunostained for RyR1, γ_{cyto}-actin, and F-actin (A) and SERCA1, Tmod4, and F-actin (B). M, M line; P, thin filament pointed ends; Z, Z line. Bars, 1 μm.

thin filament pointed ends in the absence of Tmod1 (Fig. 2 E). These results confirm that Tmod3 and Tmod4 rearrange and establish a structural compensatory mechanism in the absence of Tmod1. However, the amounts of Tmod3 and γ_{cyto}-actin in the 15,000- and 150,000-g pellets did not change in $Tmod1^{-/-Tg+}$ muscle. This may be because whole-muscle homogenates and their fractions are contaminated with erythrocytes (a nonmuscle source of Tmod1) and endothelial cells (a nonmuscle source of Tmod3 and γ_{cyto}-actin; Fowler, 1987, 1990; Galustian et al., 1995; Conley et al., 2001; Fischer et al., 2003). This may have skewed the distributions of Tmod1, Tmod3, and γ_{cyto}-actin in favor of the higher-speed pellets and obscured small changes in the fractionation patterns.

Deletion of Tmod1 alters the localization of sAnk1.5, a novel binding partner of Tmod3

To investigate whether the changes downstream of Tmod1 deletion (i.e., Tmod3 translocation to the thin filament pointed ends and perturbation of γ_{cyto}-actin) might cause global changes in SR cytoskeletal organization, we screened localizations of SR-associated cytoskeletal proteins. Interestingly, the only protein that we found to be systemically mislocalized in $Tmod1^{-/-Tg+}$
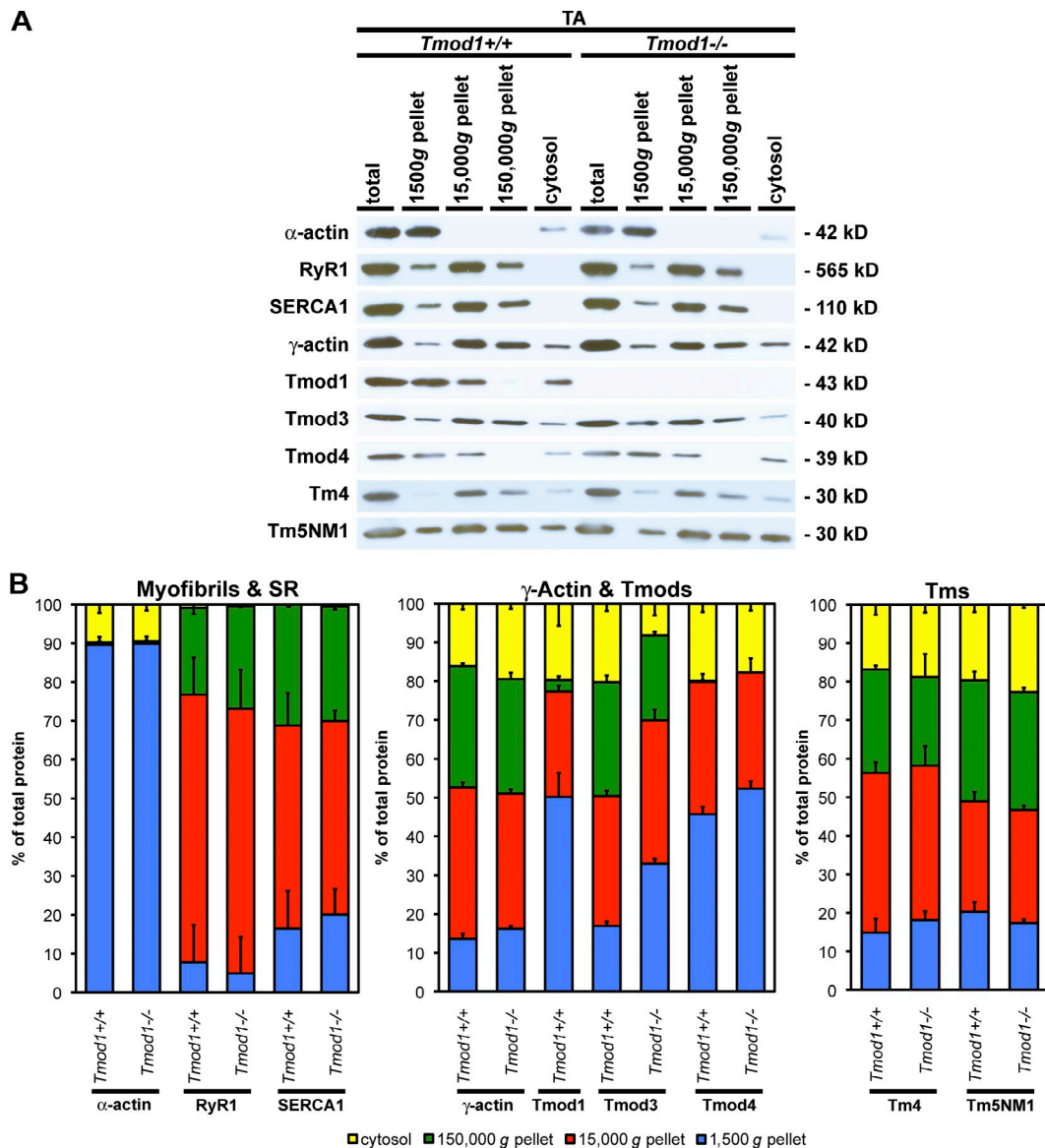
Figure 4. **Differential centrifugation of skeletal muscle proteins reveals that Tmods and γ_{cyto}-actin cofractionate with SR membranes.** (A) Western blots of TA tissue homogenate, 1,500-g pellet, 15,000-g pellet, 150,000-g pellet, and cytosol from $Tmod1^{+/+Tg+}$ and $Tmod1^{-/-Tg+}$ mice. Loading of fractions was normalized with respect to the initial volume of the total homogenate. Blots were probed for α_{sk}-actin, RyR1, SERCA1, γ_{cyto}-actin, Tmod1, Tmod3, Tmod4, Tm4, and Tm5NM1. (B) Quantitation of Western blots. Each bar reflects the mean of three independent blots. The proportions of Tmod3 in the 1,500-g and cytosolic fractions and the proportion of Tmod4 in the 1,500-g fraction were significantly different between $Tmod1^{+/+Tg+}$ and $Tmod1^{-/-Tg+}$ muscle (P < 0.05 for each). Data are presented as mean ± SD.

muscle was sAnk1.5, a 17-kD splice variant of ankyrin-R that links the SR to the M line by binding to obscurin (Bagnato et al., 2003; Kontrogianni-Konstantopoulos et al., 2003; Porter et al., 2005; Lange et al., 2009). In $Tmod1^{+/+Tg+}$ muscle, sAnk1.5 localizes predominantly to the M line as reported (Bagnato et al., 2003; Kontrogianni-Konstantopoulos et al., 2003; Lange et al., 2009), although low levels of Z line–associated sAnk1.5 could also be detected (Fig. 5 A). However, in $Tmod1^{-/-Tg+}$ muscle, sAnk1.5 immunostaining revealed a wide stripe overlaying the Z line that resembled the staining pattern of the γ_{cyto}-actin/Tmod3 SR microdomain (Fig. 5 A). This change in localization was confirmed quantitatively by an ~95% reduction in the ratio of sAnk1.5 M/Z fluorescence in $Tmod1^{-/-Tg+}$ muscle (Fig. 5 B). However, sAnk1.5 protein levels did not change in $Tmod1^{-/-Tg+}$

muscle (Figs. 5 C and S3). In contrast, obscurin (an sAnk1.5 binding partner) and ankyrin-B (a large canonical ankyrin isoform) had unchanged localizations in $Tmod1^{-/-Tg+}$ muscle, with the narrow M line and wide Z line staining patterns characteristic of the γ_{cyto}-actin/Tmod3 SR microdomain (Fig. S4) and identical to β2-spectrin (Fig. 2 C).

To understand the molecular mechanism for sAnk1.5 mislocalization in $Tmod1^{-/-Tg+}$ muscle, we performed coimmunoprecipitation (co-IP) experiments using muscle extracts. Tmod3 and γ_{cyto}-actin coimmunoprecipitated with anti-sAnk1.5–coated beads, and, in an inverse experiment, sAnk1.5 and γ_{cyto}-actin coimmunoprecipitated with anti-Tmod3–coated beads (Fig. 5 D). Tmod1 and sAnk1.5 did not coimmunoprecipitate with anti-sAnk1.5– and anti-Tmod1–coated beads, respectively (Fig. 5 D),
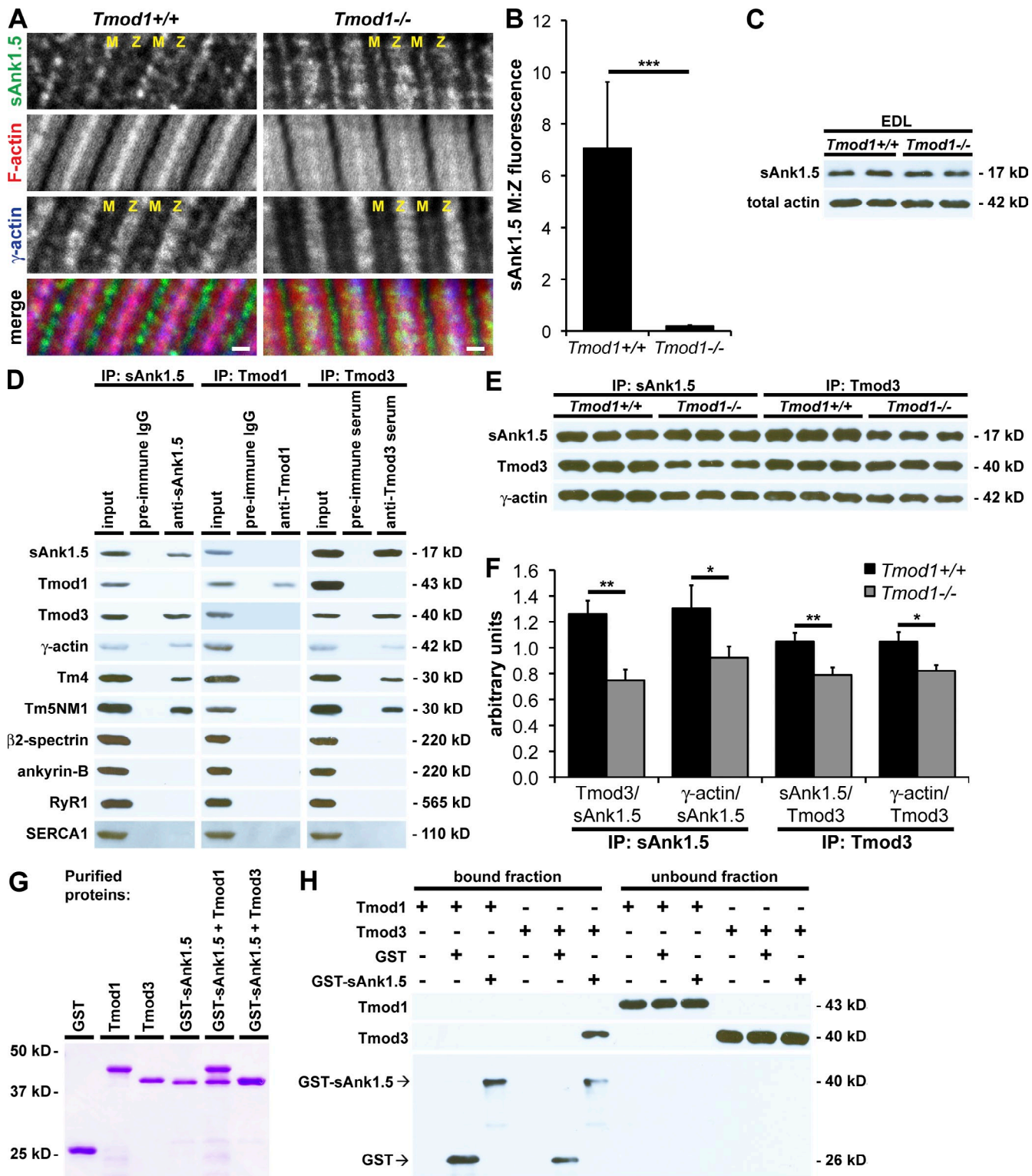
Figure 5. **Tmod3 and γ_{cyto}-actin form a complex with sAnk1.5, which appears at the Z line in the absence of Tmod1.** (A) Longitudinal cryosections of 1-mo-old TA muscle fibers from $Tmod1^{+/+Tg+}$ and $Tmod1^{-/-Tg+}$ mice immunostained for γ_{cyto}-actin, F-actin, and sAnk1.5. M, M line; Z, Z line. Bars, 1 μm. (B) Quantitation of the ratio of M/Z fluorescence of sAnk1.5. Each bar reflects n = 59–63 myofibrils/genotype measured from three mice (six muscles)/genotype. Data are presented as mean ± SD. ***, $P < 0.001$. (C) Western blots of EDL tissue lysates show no changes in sAnk1.5 levels in $Tmod1^{-/-Tg+}$ mice. (D) Western blots of clarified muscle extract (input) coimmunoprecipitated using antibodies against sAnk1.5, Tmod1, or Tmod3 or their respective negative controls. Note the co-IP of Tmod3, γ_{cyto}-actin, nonmuscle Tms, and sAnk1.5 but not Tmod1, β2-spectrin, ankyrin-B, RyR1, or SERCA1. (E) Western blots of clarified muscle extract coimmunoprecipitated using antibodies against sAnk1.5 or Tmod3 show reduced co-IP of sAnk1.5, Tmod3, and γ_{cyto}-actin in $Tmod1^{-/-Tg+}$ muscle. (F) Quantitation of sAnk1.5, Tmod3, and γ_{cyto}-actin protein ratios in coimmunoprecipitated $Tmod1^{+/+Tg+}$ and $Tmod1^{-/-Tg+}$ muscle extract. Each bar reflects n = 3 lanes. Data are presented as mean ± SD. *, $P < 0.05$; **, $P < 0.01$. (G) Coomassie-stained gel of purified proteins used for GST pull-down experiments. (H) Western blots of bound and unbound fractions of Tmod1 or Tmod3 pulled down by glutathione resin alone or resin loaded with GST or GST-sAnk1.5.
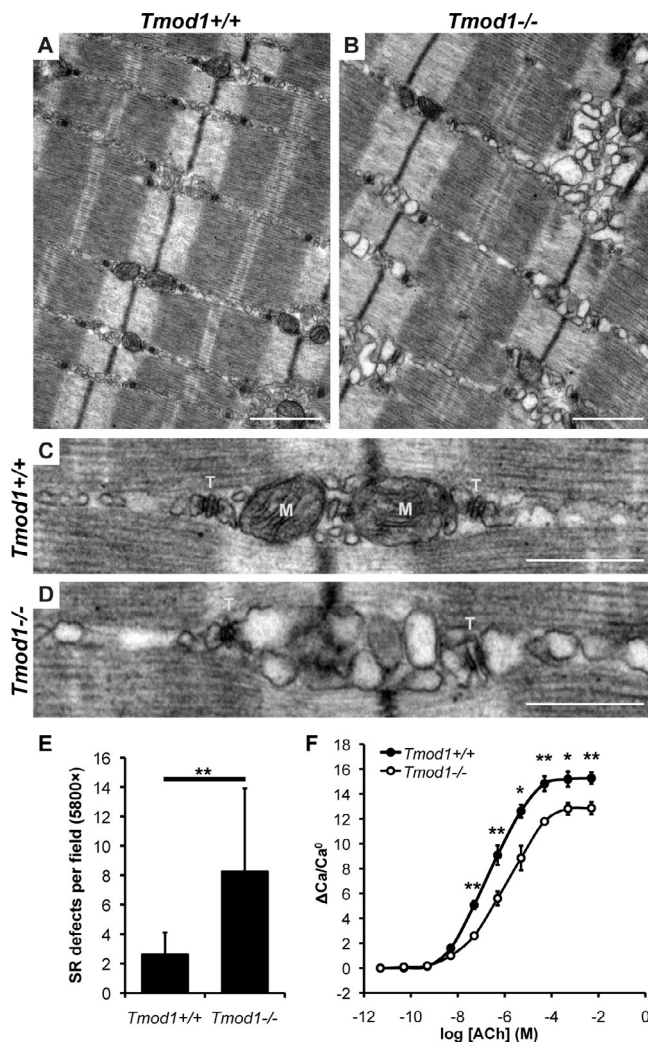
Figure 6. **Deletion of Tmod1 produces ultrastructural defects in the SR and depresses SR Ca²⁺ release.** (A and B) TEM of 6-mo-old longitudinal EDL muscle sections from $Tmod1^{+/+Tg+}$ (A) and $Tmod1^{-/-Tg+}$ (B) mice. Bars, 1 µm. (C and D) Higher-magnification TEM of the SR of $Tmod1^{+/+Tg+}$ (C) and $Tmod1^{-/-Tg+}$ (D) muscle. M, mitochondria; T, triads. Bars, 0.5 µm. (E) Quantitation of SR defects in $Tmod1^{+/+Tg+}$ and $Tmod1^{-/-Tg+}$ EDL muscle at 5,800× magnification. Each bar reflects n = 20 images/genotype from two mice (four muscles)/genotype. (F) Ca²⁺ flux as a function of ACh concentration for $Tmod1^{+/+Tg+}$ and $Tmod1^{-/-Tg+}$ TA fiber suspensions. Note the reduced Ca²⁺ flux in $Tmod1^{-/-Tg+}$ fibers. Each data point reflects the mean of four independent experiments. Data are presented as mean ± SD. *, P < 0.01; **, P < 0.001.

indicating that Tmod participation in this complex is Tmod3 specific. Moreover, neither β2-spectrin, ankyrin-B, RyR1, nor SERCA1 coimmunoprecipitated with either sAnk1.5 or Tmod3 (Fig. 5 D). Thus, sAnk1.5, Tmod3, and γ_{cyto}-actin establish a novel SR-associated protein complex at the M line. Comparison of co-IPs from $Tmod1^{-/-Tg+}$ and $Tmod1^{+/+Tg+}$ muscles showed that less Tmod3 and γ_{cyto}-actin were associated with anti-sAnk1.5–coated beads and, similarly, that less sAnk1.5 and γ_{cyto}-actin were associated with anti-Tmod3–coated beads (Figs. 5 [E and F] and S5). Thus, the Tmod3–γ_{cyto}-actin–sAnk1.5 complex partially dissociates when Tmod3 leaves the SR and translocates to the thin filament pointed ends in the absence of Tmod1. Furthermore, GST-sAnk1.5 pull-down experiments revealed

that Tmod3 (but not Tmod1) binds directly to sAnk1.5 (Fig. 5, G and H). The sAnk1.5–Tmod3 interaction may be weak in vitro, as most of the Tmod3 incubated with GST-sAnk1.5 remained in the unbound fraction (Fig. 5 H). Regardless, direct binding of Tmod3 to GST-sAnk1.5 and co-IP of Tmod3 and γ_{cyto}-actin from muscle extracts with sAnk1.5 antibodies demonstrate that Tmod3 and γ_{cyto}-actin can establish direct cytoskeletal linkages to the SR via a specific SR constituent, sAnk1.5.

The SR is structurally and functionally compromised in the absence of Tmod1

To investigate whether the absence of Tmod1, translocation of Tmod3, disruption of γ_{cyto}-actin, and mislocalization of sAnk1.5 might be accompanied by morphological changes in the SR, we performed transmission EM (TEM) on $Tmod1^{+/+Tg+}$ and $Tmod1^{-/-Tg+}$ muscle. This revealed pathological swelling of the SR in $Tmod1^{-/-Tg+}$ muscle that was comparatively rare in $Tmod1^{+/+Tg+}$ muscle (Fig. 6, A and B). Closer examination of these defects revealed swollen, electron-lucent SR vesicles between myofibrils, particularly in the vicinity of Z lines (Fig. 6, C and D). Z lines and triads tended to be displaced from the regions containing swollen SR, although triad morphology appeared normal (Fig. 6, A–D). Occasional instances of mitochondrial swelling were also observed but were not significantly more abundant (0.90 ± 0.85 vs. 1.20 ± 1.15 mitochondrial defects/5,800× field in $Tmod1^{+/+Tg+}$ vs. $Tmod1^{-/-Tg+}$ muscle, respectively; P = 0.36). SR defects were approximately three-fold more prevalent in $Tmod1^{-/-Tg+}$ muscle than in $Tmod1^{+/+Tg+}$ muscle (Fig. 6 E), although the frequency of SR defects in $Tmod1^{-/-Tg+}$ muscle was quite variable (coefficient of variation = 0.68). SR defects were focal, and the majority of the SR was intact in $Tmod1^{-/-Tg+}$ muscle, which may explain why RyR1 and SERCA1 immunofluorescence appeared normal in $Tmod1^{-/-Tg+}$ muscle (Fig. 3) despite the large number of SR defects evident by TEM. To determine whether these defects adversely impact SR Ca²⁺ handling, we used a fluorescence-based Ca²⁺ flux assay to compare SR Ca²⁺ release in suspensions of TA muscle fibers immediately after cholinergic stimulation by exogenous acetylcholine (ACh). Peak ACh-induced Ca²⁺ flux in $Tmod1^{-/-Tg+}$ muscle fibers was reduced by ∼15% compared with $Tmod1^{+/+Tg+}$ fibers (Fig. 6 F), indicating defective Ca²⁺ release, which is consistent with SR defects in the absence of Tmod1. Therefore, the absence of Tmod1, translocation of Tmod3, and disruption of γ_{cyto}-actin produce defects in both the structure and function of the SR.

Deletion of Tmod1 perturbs nonmuscle Tms in skeletal muscle

Nonmuscle Tm4 and Tm5NM1 play important physiological roles in regulating SR morphology and excitation–contraction coupling in skeletal muscle (Kee et al., 2004; Vlahovich et al., 2008, 2009). The abnormal SR morphology and the loss of γ_{cyto}-actin from the M line in the absence of Tmod1 led us to ask whether nonmuscle Tm4 and Tm5NM1 are perturbed in the absence of Tmod1. Immunostaining of longitudinal sections of $Tmod1^{+/+Tg+}$ and $Tmod1^{-/-Tg+}$ muscle revealed that both Tm4 and Tm5NM1 localize to stripes at the M line and flanking the
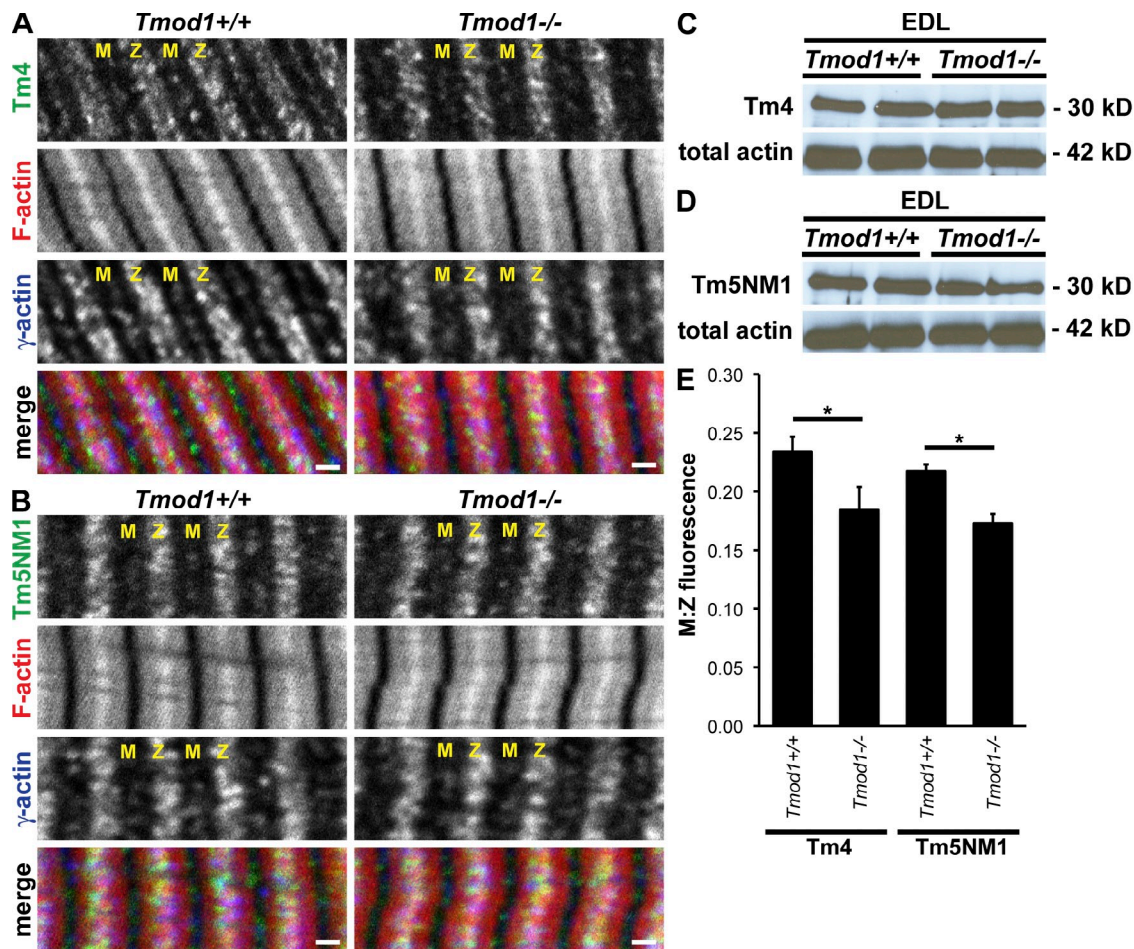
Figure 7. **Deletion of Tmod1 depletes nonmuscle Tms from the M line.** (A and B) Longitudinal cryosections of 1-mo-old TA muscle fibers from $Tmod1^{+/+Tg+}$ and $Tmod1^{-/-Tg+}$ mice immunostained for γ_{cyto}-actin, F-actin, and either Tm4 (A) or Tm5NM1 (B). M, M line; Z, Z line. Bars, 1 µm. (C and D) Western blots of EDL tissue lysates show no changes in Tm4 (C) and Tm5NM1 (D) levels in $Tmod1^{-/-Tg+}$ muscle. (E) Quantitation of M/Z fluorescence of Tms. Each bar reflects n = 52–61 myofibrils/genotype measured from three mice (six muscles)/genotype. Data are presented as mean ± SD. *, $P < 0.001$.

Z line, similar to γ_{cyto}-actin (Fig. 7, A and B). Western blotting did not show any changes in the levels of Tm4 and Tm5NM1 in $Tmod1^{-/-Tg+}$ muscle (Figs. 7 [C and D] and S3). However, for both Tm4 and Tm5NM1, the ratio of M/Z fluorescence was ~0.23 in $Tmod1^{+/+Tg+}$ muscle, decreasing by ~25% to ~0.18 in $Tmod1^{-/-Tg+}$ muscle (Fig. 7 E), which was strikingly similar to the redistribution of γ_{cyto}-actin (Fig. 2 D). Therefore, the deletion of Tmod1 results in redistribution of nonmuscle Tms from the M line to the Z line, paralleling γ_{cyto}-actin. Both Tm4 and Tm5NM1 cofractionated with γ_{cyto}-actin and Tmod3 in the 15,000- and 150,000-g pellets, similar to SR markers, and a larger proportion of Tm4 than Tm5NM1 was associated with the 15,000-g pellet (~41 vs. ~29%, respectively), which was unchanged in $Tmod1^{-/-Tg+}$ muscle (Fig. 4). Most likely, the perturbation of nonmuscle Tms revealed by immunofluorescence may have been insufficient to change the relative proportions of the nonmuscle Tms in the SR-associated fractions. Alternatively, contamination of the muscle homogenates by nonmuscle cells may have suppressed our ability to detect changes in the sorting of Tm isoforms across muscle compartments in the absence of Tmod1, similar to the case of γ_{cyto}-actin. Furthermore, both Tm4 and Tm5NM1 coimmunoprecipitated with sAnk1.5,

Tmod3, and γ_{cyto}-actin but not with Tmod1 (Fig. 5 D). Thus, nonmuscle Tms are associated with the γ_{cyto}-actin/Tmod3 SR microdomain in skeletal muscle, including the M line Tmod3–sAnk1.5 complex, where they presumably stabilize γ_{cyto}-actin filaments by binding along their sides and interacting with Tmods at γ_{cyto}-actin pointed ends.

Deletion of Tmod1 increases sarcomere misalignment but does not perturb desmin or the DGC

Intact cytoskeletal connections among core myofibrils, peripheral myofibrils, and sarcolemma are important for maintaining sarcomere alignment and providing efficient lateral force transmission during muscle contraction (Monti et al., 1999; Shah et al., 2004; Meyer et al., 2010). Because γ_{cyto}-actin perturbation, Tmod3 translocation, and sAnk1.5 mislocalization in the absence of Tmod1 produce defects in the SR in the vicinity of the Z line, we used TEM of 1- and 6-mo-old muscles to examine whether $Tmod1^{-/-Tg+}$ muscles exhibit elevated sarcomere misalignment. TEM revealed a small and age-dependent increase in sarcomere misalignment in $Tmod1^{-/-Tg+}$ extensor digitorum longus (EDL) muscle, as determined by normalizing longitudinal
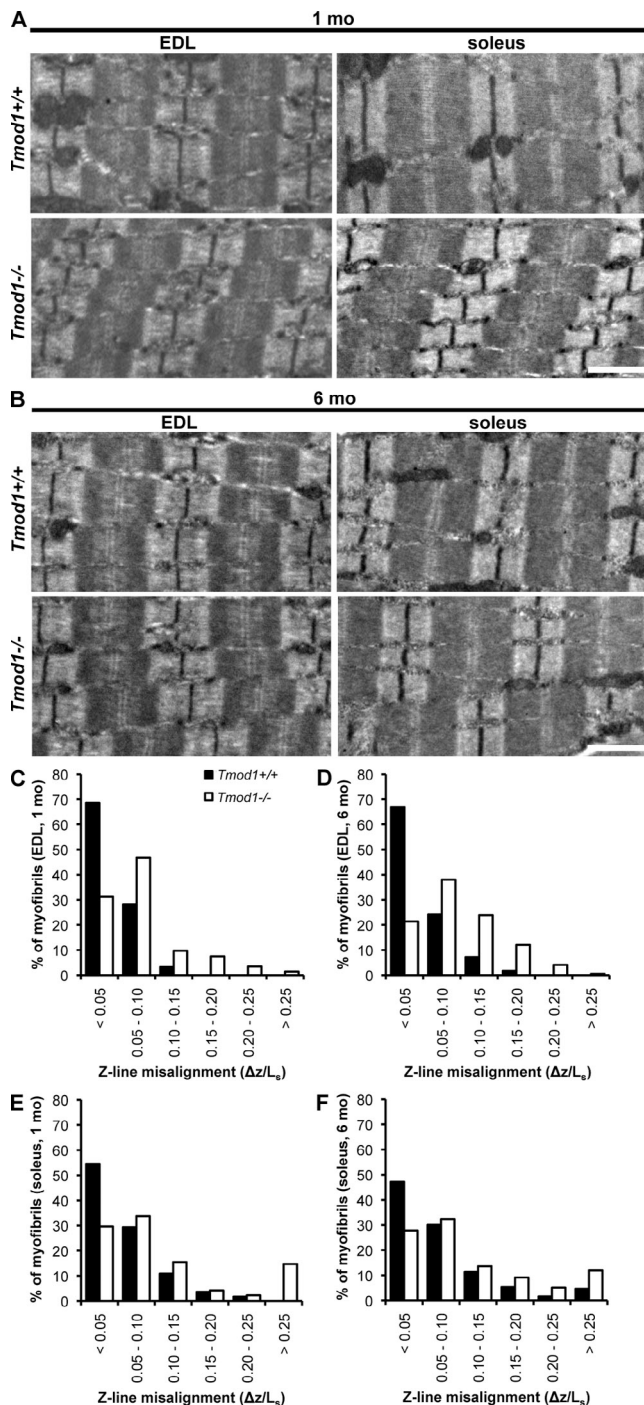
Figure 8. **Deletion of Tmod1 produces an age-dependent increase in sarcomere misalignment.** (A and B) TEM of 1- (A) and 6-mo-old (B) longitudinal EDL muscle sections from $Tmod1^{+/+Tg+}$ and $Tmod1^{-/-Tg+}$ mice. Bars, 1 µm. (C–F) Frequency distribution of $\Delta z/L_s$ in EDL (C and D) and soleus (E and F) muscles from 1- (C and E) and 6-mo-old (D and F) $Tmod1^{+/+Tg+}$ and $Tmod1^{-/-Tg+}$ mice. Each distribution reflects $n = 34$–72 myofibrils/genotype for 1-mo-old mice and $n = 239$–881 myofibrils/genotype for 6-mo-old mice measured from two mice/age/genotype (four muscles/age/genotype), which were collected in a single experiment.

Z line offset to sarcomere length ($\Delta z/L_s$; Fig. 8, A–D). Sarcomere misalignment was more pronounced in $Tmod1^{-/-Tg+}$ soleus muscle, with ~15% of myofibrils exhibiting $\Delta z/L_s > 0.25$, although myofibril misalignment in the soleus was less age-

dependent than in the EDL (Fig. 8, A, B, E, and F). Because the soleus is a slower and more heavily recruited muscle than the EDL, the magnitude of sarcomere misalignment in the absence of Tmod1 is muscle type dependent. Thus, the fortification of the SR by γ_{cyto}-actin, Tmod3, sAnk1.5, and nonmuscle Tms plays a novel role in maintaining the alignment of adjacent myofibrils during muscle contraction and use.

Elevated sarcomere misalignment in $Tmod1^{-/-Tg+}$ muscle led us to ask whether the organization of the desmin intermediate filament network, which is known to mechanically align myofibrils (Milner et al., 1996; Shah et al., 2002, 2004; Meyer et al., 2010), might be altered in the absence of Tmod1. Desmin levels were unchanged in $Tmod1^{-/-Tg+}$ muscle (Figs. 9 A and S3), and no obvious changes in desmin localization were identified in $Tmod1^{-/-Tg+}$ muscle, with desmin localizing to Z lines and more faintly to M lines in both genotypes (Fig. 9 D). Desmin transmits contractile force to the sarcolemma by interacting with its binding partners at the costamere, which is composed of the DGC and other subcomplexes. The DGC is anchored by the giant protein dystrophin, an integral costamere constituent and γ_{cyto}-actin–binding protein (Renley et al., 1998; Rybakova et al., 2000). Therefore, we examined whether γ_{cyto}-actin alterations in the absence of Tmod1 might perturb the DGC. We found no changes in β-dystroglycan or dystrophin levels (Figs. 9 [B and C] and S3) or localization (Fig. 9 E) in $Tmod1^{-/-Tg+}$ muscle. This, and the fact that skeletal muscle–specific deletion of γ_{cyto}-actin has no effect on the DGC (Sonnemann et al., 2006), indicates that neither normal Tmod1 levels nor correct pointed end regulation of extrasarcomeric γ_{cyto}-actin by Tmod1 is required for assembly and targeting of the DGC to the sarcolemma.

Discussion

Tmods and γ_{cyto}-actin stabilize the SR

We have identified two distinct SR-associated compartments that contain γ_{cyto}-actin and its binding partners. The first has a narrow M line and wide Z line–flanking signature and contains Tmod3, γ_{cyto}-actin, nonmuscle Tms, β2-spectrin, ankyrin-B, and obscurin, whereas the second has a narrow Z line–flanking doublet signature and contains Tmod1 and Tmod4. The first γ_{cyto}-actin compartment has a similar staining pattern as SERCA1, whereas the second γ_{cyto}-actin compartment resembles the narrow RyR1 doublets flanking the Z line but not at the M line. We propose that, in $Tmod1^{+/+Tg+}$ muscle, extrasarcomeric γ_{cyto}-actin pointed ends are predominantly capped by Tmod3, with smaller contributions from Tmod1 and Tmod4 (this study), whereas Tmod1 and Tmod4 cap thin filament pointed ends (Gokhin et al., 2010). Tmod3 may regulate SR-associated γ_{cyto}-actin by inhibiting the dissociation of actin monomers from pointed ends, stabilizing filaments and linking γ_{cyto}-actin filament pointed ends to the SR membrane via Tmod3 binding to sAnk1.5 (Fig. 10). SR-associated γ_{cyto}-actin filaments may be further stabilized by the binding of nonmuscle Tm4 and Tm5NM1, similar to Tmods in other actin filament systems (Weber et al., 2007; Nowak et al., 2009; Moyer et al., 2010). In $Tmod1^{-/-Tg+}$ muscle, Tmod1 is absent from the SR, and Tmod3 redistributes from the SR to the thin filament pointed ends in sarcomeres, thus destabilizing
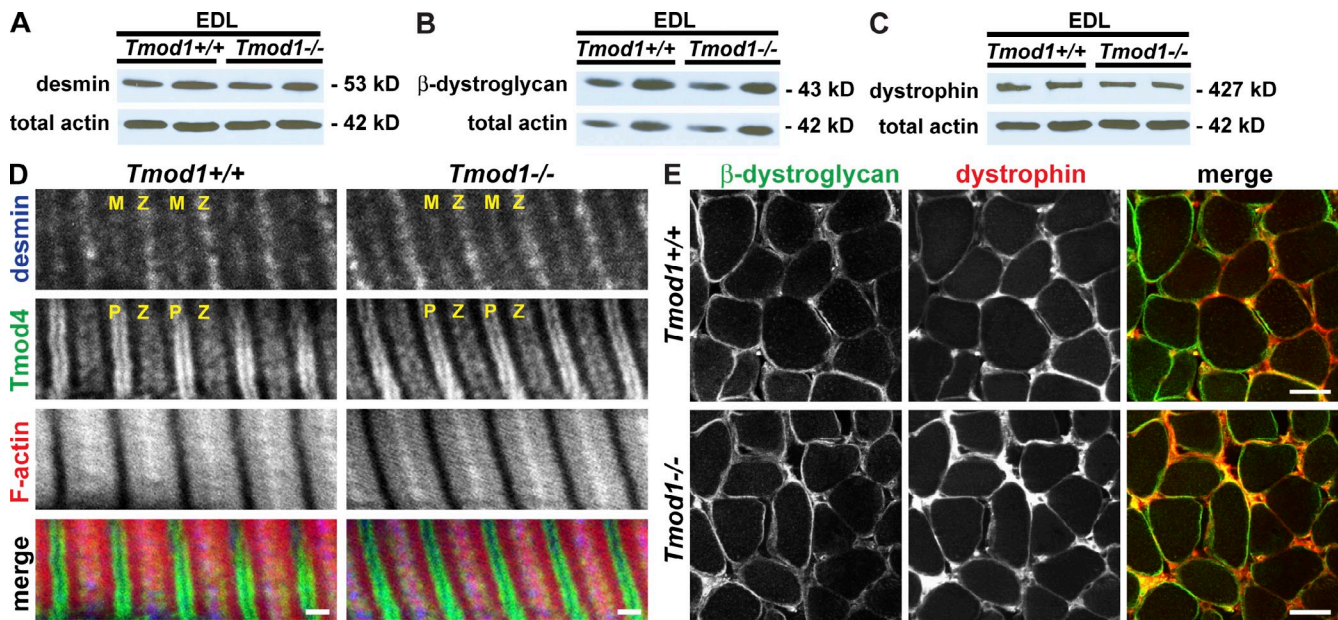
Figure 9. **Intact desmin intermediate filament network and DGC in the absence of Tmod1.** (A–C) Western blots of EDL tissue lysates show no changes in desmin (A), β-dystroglycan (B), and dystrophin (C) levels in $Tmod1^{-/-Tg+}$ mice. (D) Longitudinal cryosections of 1-mo-old TA muscle fibers from $Tmod1^{+/+Tg+}$ and $Tmod1^{-/-Tg+}$ mice immunostained for desmin, Tmod4, and F-actin. M, M line; P, thin filament pointed ends; Z, Z line. Bars, 1 µm. (E) Transverse cryosections of 1-mo-old TA muscle fibers from $Tmod1^{+/+Tg+}$ and $Tmod1^{-/-Tg+}$ mice immunostained for β-dystroglycan and dystrophin. Bars, 25 µm.

the SR-associated γ_{cyto}-actin complex of Tmod3, Tm4, and Tm5NM1 with sAnk1.5 (Fig. 10). The loss of γ_{cyto}-actin–mediated connectivity in $Tmod1^{-/-Tg+}$ muscle may mechanically weaken the SR, producing aberrant SR swelling and depressed Ca^{2+} release. The disruption of linkages between the SR and myofibrils could then cause myofibril misalignment that becomes more pronounced as muscles are recruited more frequently, thereby imposing chronic mechanical stress on a structurally compromised cytoskeletal network.

Our findings provide a mechanism that can explain the physiological alterations in $Tmod1^{-/-Tg+}$ muscle. We have shown previously that absence of Tmod1 does not alter thin filament lengths because of structural compensation by Tmod3 and Tmod4 (Gokhin et al., 2010). Even though thin filament lengths are normal in $Tmod1^{-/-Tg+}$ muscle, $Tmod1^{-/-Tg+}$ muscle still exhibits depressed isometric stress production (Gokhin et al., 2010). We propose that a combination of defects in Ca^{2+} release and lateral force transmission underlies this functional deficit. Our Ca^{2+} flux assays show that SR defects in the absence of Tmod1 lead to inadequate Ca^{2+} release and incomplete thin filament activation. Furthermore, when γ_{cyto}-actin and the SR are disrupted in the absence of Tmod1, adjacent myofibrils become mechanically decoupled, leading to myofibril misalignment and a likely depression in the net force transmitted to the cell exterior. Either mechanism can produce a muscle phenotype whereby depressed isometric stress production and locomotor behavior lead to fiber-type reprogramming that reflects decreased use (Gokhin et al., 2010).

Skeletal muscle fibers contain a nonmuscle-like, SR-associated cytoskeleton

Membrane adaptors such as ankyrins link spectrin–actin networks and spectrin-based membrane skeletons to membrane

proteins, including SR-associated ion channels in striated muscle (Bennett and Healy, 2008; Cunha and Mohler, 2009). Our data implicate Tmods as a novel class of molecules that compartmentalize the skeletal muscle SR via linkages to sAnk1.5 at the M line. sAnk1.5 is a 17-kD skeletal muscle–specific splice variant of ankyrin-R (Ank1) that lacks the N-terminal tandem repeat and spectrin-binding domains of canonical ankyrins and, in their place, contains a unique 73–amino acid–long N-terminal domain with a 22-residue hydrophobic membrane-binding sequence (Gallagher et al., 1997; Gallagher and Forget, 1998; Porter et al., 2005). Our co-IP and immunostaining results show that Tmod3, γ_{cyto}-actin, and nonmuscle Tms form a complex with sAnk1.5 at the M line that is distinct from β2-spectrin or ankyrin-B complexes and that does not contain SERCA1 or RyR1. sAnk1.5 is targeted to the M line by binding to obscurin, a giant protein that is anchored to myomesin and titin in the thick filaments (Fukuzawa et al., 2008). We propose that Tmod3 binding to obscurin-tethered sAnk1.5 recruits γ_{cyto}-actin and nonmuscle Tms to an SR microdomain at the M line. In this event, Tmod3 may interact with a site on sAnk1.5 distinct from its obscurin-binding site (Borzok et al., 2007). However, because obscurin remains at the M line in the absence of Tmod1, yet sAnk1.5 mislocalizes to the Z line when Tmod3 translocates to thin filament pointed ends, additional factors may anchor Tmod3 and sAnk1.5 to the M line SR compartment. Obscurin-null muscle also exhibits sAnk1.5 mislocalization to the Z line along with retraction of the longitudinal SR toward the Z line (Lange et al., 2009), but SR retraction is not observed in Tmod1-null muscle (Figs. 6 and 8). Regardless, mislocalization of sAnk1.5 when Tmod3 vacates the M line in the absence of Tmod1 argues that the secondary rearrangement of Tmod3 in the absence of Tmod1 induces systemic SR alterations in $Tmod1^{-/-Tg+}$ muscle.
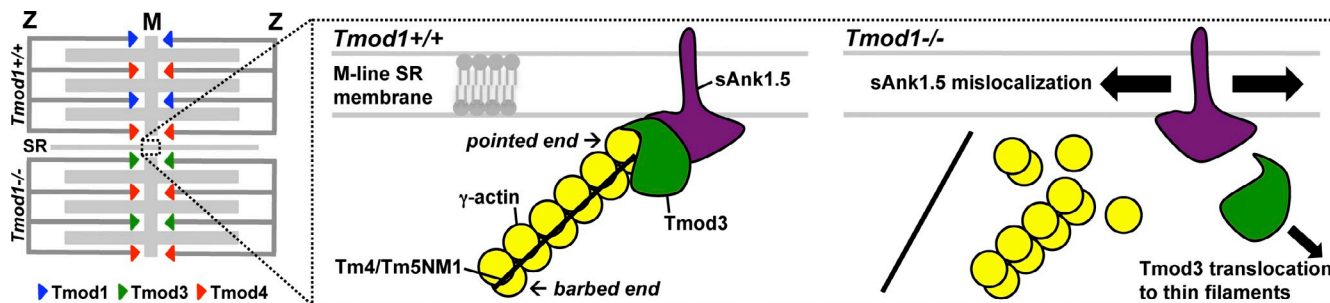
Figure 10. **Model of thin filament pointed end capping by Tmods and organization of the M line SR Tmod3–γ_{cyto}-actin–sAnk1.5 complex in *Tmod1*[+/+Tg+]** **and *Tmod1*[−/−Tg+] muscle.** In *Tmod1*[+/+Tg+] muscle, thin filament pointed ends are capped by a combination of Tmod1 and Tmod4, whereas Tmod3 is predominantly associated with the SR. In *Tmod1*[−/−Tg+] muscle, Tmod3 translocates from the SR to the thin filament pointed ends, destabilizing the Tmod3–γ_{cyto}-actin–sAnk1.5 complex. M, M line; Z, Z line.

However, the normal localizations of RyR1 and SERCA1 and the focal SR defects in *Tmod1*[−/−Tg+] muscle argue that defects may simply occur in focal sites of elevated mechanical stress that arise during muscle contraction and use.

The role that Tmod3 plays in organizing extrasarcomeric γ_{cyto}-actin in the SR is analogous to the roles that Tmods play in lens fiber cells and erythrocytes, in which deletion of Tmod1 results in misregulation of membrane-associated F-actin, reduced Tm–F-actin association, and perturbation of the spectrin-based membrane skeleton, manifested physiologically as defects in cell morphology and mechanics (Nowak et al., 2009; Moyer et al., 2010). A similar result is observed in confluent cultures of polarized epithelial cells, in which short hairpin RNA–mediated knockdown of Tmod3 results in the loss of F-actin and Tm from lateral membranes, disruption of α2-spectrin, and reduction in cell height (Weber et al., 2007). In contrast to the aforementioned studies, the M line Tmod3–γ_{cyto}-actin–sAnk1.5 complex lacks β2-spectrin. Although the existence of Tmod–actin structures lacking spectrin has precedent in the lens (Woo et al., 2000), spectrin may be absent from the Tmod3–γ_{cyto}-actin–sAnk1.5 complex detected by co-IP because radioimmunoprecipitation assay (RIPA) buffer depolymerizes F-actin (unpublished data), thus eliminating β2-spectrin's F-actin attachment points, leaving only the proteins at the pointed ends of the filaments in the complex. Regardless, the sorting of γ_{cyto}-actin and Tmods into extrasarcomeric SR microdomains identifies the SR as a new entry in the list of biological membrane systems whose architecture and physiology are regulated by Tmods.

Thus far, the molecular basis for the differential compartmentalization of α_{sk}-actin and γ_{cyto}-actin with Tmods is unclear. These actins share 93% sequence identity; their little divergence is chiefly in their eight extreme N-terminal residues in actin subdomain I. Experiments using in vitro chemical cross-linking of Tmod3 and α_{sk}-actin identified residues on subdomains I and II of actin that directly interact with Tmod3 (Yamashiro et al., 2010). Of these residues, D24, D25, E99, and E100 are in actin subdomain I and conserved in all actin isoforms, close to actin's divergent extreme N terminus (Otterbein et al., 2001), which therefore might function as a cap mediator, either enhancing or inhibiting Tmod isoform binding to subdomain I. In muscle cells, the N terminus of γ_{cyto}-actin might recruit Tmod3 to the SR cytoskeleton, whereas the N terminus of α_{sk}-actin might

facilitate Tmod1 and Tmod4 binding to thin filament pointed ends. Alternatively, binding of Tmod3 to sAnk1.5 could specifically target Tmod3 and γ_{cyto}-actin filaments to the SR. Either mechanism is consistent with the phenotype of *Tmod1*[−/−Tg+] muscle (Gokhin et al., 2010; this study), in which Tmod–actin isoform interactions in skeletal muscle appear to be biochemically tuned in a manner that prioritizes α_{sk}-actin thin filament length regulation over γ_{cyto}-actin regulation. Such actin isoform–specific biochemistry likely arises from differential molecular interactions of various combinations of actins, Tmods, and Tms.

Multiple cytoskeletal systems align adjacent myofibrils

Maintaining alignment among adjacent myofibrils is a function that has canonically been ascribed to desmin intermediate filaments (Milner et al., 1996; Shah et al., 2002, 2004; Meyer et al., 2010). Because the absence of Tmod1 and the translocation of Tmod3 lead to a reorganization of intermyofibrillar γ_{cyto}-actin, sAnk1.5 mislocalization, SR defects, and increased sarcomere misalignment, the SR membrane itself, mechanically fortified by γ_{cyto}-actin, is involved in aligning myofibrils. By tethering together adjacent myofibrils, the SR can reduce intermyofibrillar sliding during muscle deformation. Previous data have suggested that the C terminus of nebulin may act as a bridge between desmin and α_{sk}-actin at the Z line and that desmin binding to nebulin mediates both thin filament lengths and myofibril alignment (Bang et al., 2002; Conover et al., 2009; Tonino et al., 2010). However, thus far, there is no evidence for a similar protein bridge between desmin and γ_{cyto}-actin in the SR. Because the absence of Tmod1 does not perturb the desmin intermediate filament system (this study) or the localizations of the N and C termini of nebulin (Gokhin et al., 2010), these cytoskeletal systems appear to be decoupled in terms of their biochemistry while remaining homologous in terms of their function. It is appealing to speculate that redundant and functionally homologous protein systems evolved as a fail-safe mechanism to ensure correct striated muscle function.

Implications for the phenotypes of mice with altered γ_{cyto}-actin levels

Based on its strategic enrichment at costameres, interaction with dystrophin, and dramatic up-regulation in dystrophic muscles,

extrasarcomeric γ_{cyto}-actin has been thought to play a stabilizing and/or force-transmitting role at the sarcolemma (Craig and Pardo, 1983; Renley et al., 1998; Rybakova et al., 2000; Hanft et al., 2006, 2007). However, experiments involving targeted genetic perturbation of γ_{cyto}-actin expression in skeletal muscle have produced inconsistent results. Skeletal muscle–specific deletion of γ_{cyto}-actin produces functional deficits, corroborating a role in muscle function (Sonnemann et al., 2006), but the deletion of γ_{cyto}-actin from *mdx* muscle does not increase the severity of the *mdx* phenotype, which makes the surprising suggestion that the stabilization of the dystrophic sarcolemma by γ_{cyto}-actin may actually be dispensable (Prins et al., 2008). Also surprising is that 2,000-fold overexpression of γ_{cyto}-actin and resultant γ_{cyto}-actin incorporation into thin filaments do not appear to have any obvious effects on muscle structure or performance (Jaeger et al., 2009). SR defects and increased sarcomere misalignment arising from the absence of Tmod1, translocation of Tmod3, disruption of γ_{cyto}-actin, and mislocalization of sAnk1.5 predict that outright deletion of γ_{cyto}-actin might also produce a similar phenotype. Our data are the first to show that any actin-binding protein regulates SR-associated γ_{cyto}-actin and sAnk1.5 in skeletal muscle and that this regulation stabilizes the SR and aligns adjacent myofibrils. Elucidation of γ_{cyto}-actin dynamics, stability, and architecture in the context of its regulatory proteins may reconcile the inconsistent results of γ_{cyto}-actin under- and overexpression experiments.

Materials and methods

Experimental animals
The embryonic lethality of Tmod1-null mice was previously rescued with a Tmod1 transgene controlled by the cardiac α-MHC promoter (*Tg(α-MHC–Tmod1)*, denoted as *Tg+* in the text; McKeown et al., 2008). Tmod1-null mice with the *Tg(α-MHC–Tmod1)* transgene express Tmod1 exclusively in the heart and in no other tissues and survive into adulthood (McKeown et al., 2008; Nowak et al., 2009; Gokhin et al., 2010; Moyer et al., 2010). In immunofluorescence and whole-muscle Western blot experiments, 1-mo-old *Tmod1$^{+/+Tg+}$* and *Tmod1$^{-/-Tg+}$* mice were sacrificed by halothane inhalation followed by cervical dislocation. For TEM, 1- and 6-mo-old mice were used. In muscle fractionation experiments, 6-mo-old mice were used. For Ca^{2+} release assays, 9-mo-old mice were used. Genotyping was performed by PCR as previously described (McKeown et al., 2008). All procedures were performed in accordance with animal care guidelines enforced by the Institutional Animal Care and Use Committee at The Scripps Research Institute.

Antibodies
For immunostaining, the primary antibodies and dilutions used were as follows: 1 µg/ml affinity-purified rabbit polyclonal anti–human Tmod1 (R1749), rabbit polyclonal antiserum to human Tmod3 (R5168bl3c, 1:100), rabbit polyclonal antiserum to chicken Tmod4 preadsorbed by passage through a Tmod1 Sepharose column (R3577bl3c, 1:25), 0.93 µg/ml affinity-purified rabbit polyclonal anti–γ_{cyto}-actin (7577; a gift from J.M. Ervasti, University of Minnesota, Minneapolis, MN), rabbit polyclonal anti–β-dystroglycan (H-242, 1:50; Santa Cruz Biotechnology, Inc.), rabbit polyclonal anti-RyR1 (AB9078, 1:100; Millipore), rabbit polyclonal anti-Tm4 (AB5449, 1:100; Millipore), 1 µg/ml rabbit polyclonal anti-sAnk1.5 (ARP42566_T100; Aviva Systems Biology), 4.4 µg/ml rabbit polyclonal anti–ankyrin-B (a gift from V. Bennett, Duke University, Durham, NC; Mohler et al., 2005), rabbit polyclonal antiobscurin (IQ-54, 1:100; a gift from S. Lange, University of California, San Diego, La Jolla, CA), sheep polyclonal anti-Tm5NM1 (AB5447, 1:100; Millipore), mouse monoclonal anti–β2-spectrin (42/B, 1:200; BD), mouse monoclonal anti-SERCA1 (VE121G9, 1:100; Santa Cruz Biotechnology, Inc.), mouse monoclonal antidystrophin (Dys2, 1:20; Millipore), mouse monoclonal antidesmin (DE-U-10, 1:100; Santa Cruz Biotechnology, Inc.), and mouse monoclonal

anti–γ_{cyto}-actin (A8481, 1:50; Sigma-Aldrich). Secondary antibodies and dilutions were as follows: Alexa Fluor 488–conjugated goat anti–rabbit IgG (1:200; Invitrogen), Alexa Fluor 488–conjugated donkey anti–sheep IgG (1:200; Invitrogen), Alexa Fluor 568–conjugated goat anti–mouse IgG (1:200; Invitrogen), Alexa Fluor 647–conjugated goat anti–mouse IgG (1:200; Invitrogen), and Alexa Fluor 647–conjugated donkey anti–sheep IgG (1:200; Invitrogen).

For Western blotting, the primary antibodies and dilutions used were as follows: 0.01 µg/ml affinity-purified rabbit polyclonal anti–human Tmod1 (R1749), rabbit polyclonal antiserum to human Tmod3 (R5168bl3c, 1:10,000), rabbit polyclonal antiserum to chicken Tmod4 preadsorbed by passage through a Tmod1 Sepharose column (R3577bl3c, 1:250), 0.02 µg/ml rabbit polyclonal anti–γ_{cyto}-actin (7577), rabbit polyclonal anti–β-dystroglycan (H-242, 1:1,000), rabbit polyclonal anti-RyR1 (AB9078, 1:1,000), rabbit polyclonal anti-Tm4 (AB5449, 1:1,000), 0.1 µg/ml rabbit polyclonal anti-sAnk1.5 (ARP42566_T100), 0.044 µg/ml rabbit polyclonal anti–ankyrin-B, rabbit polyclonal anti-GST (Z-5, 1:1,000; Santa Cruz Biotechnology, Inc.), sheep polyclonal anti-Tm5NM1 (AB5447, 1:1,000), mouse monoclonal anti–pan-actin (C4, 1:10,000; a gift from J.L. Lessard, University of Cincinnati, Cincinnati, OH), mouse monoclonal antidesmin (DE-U-10, 1:1,000), mouse monoclonal anti–β2-spectrin (42/B, 1:2,000), mouse monoclonal anti–α-actin (HUC1-1, 1:1,000; Santa Cruz Biotechnology, Inc.), mouse monoclonal anti–γ_{cyto}-actin (A8481, 1:1,000), mouse monoclonal anti-SERCA1 (VE121G9, 1:1,000), and mouse monoclonal antidystrophin (Dys2, 1:200). The secondary antibodies and dilutions used were HRP-conjugated donkey anti–rabbit IgG (1:10,000; Invitrogen), HRP-conjugated donkey anti–mouse IgG (1:10,000; Invitrogen), HRP-conjugated goat anti–rabbit IgG (1:10,000; Invitrogen), and HRP-conjugated goat anti–mouse IgG (1:10,000; Invitrogen).

Immunofluorescence staining and confocal imaging
Mouse hindlimbs were pinned to cork, immersed in ice-cold relaxing buffer (100 mM NaCl, 2 mM KCl, 2 mM MgCl$_2$, 6 mM K$_3$PO$_4$, 1 mM EGTA, and 0.1% glucose, pH 7.0), relaxed for 24 h at 4°C, and then fixed for 24 h at 4°C in 4% PFA in relaxing buffer. TA and soleus muscles were then excised, cryoprotected in 20% sucrose in PBS, embedded in optimal cutting temperature medium, and frozen on a metal block chilled in dry ice. Muscles were sectioned into 12-µm-thick cryosections and mounted on slides. Sections were washed in PBS + 0.1% Triton X-100 (PBST), permeabilized for 15 min in PBS + 0.3% Triton X-100, and blocked for 2 h in 4% BSA + 1% goat and/or donkey sera in PBST. Tissues were labeled with primary antibodies diluted in blocking buffer overnight at 4°C, washed in PBST, and then labeled with a fluorophore-conjugated secondary antibody mixture in blocking buffer for 2 h at RT. The secondary antibody mixture was supplemented with Hoechst 33258 (1:200; Invitrogen) and either Alexa Fluor 647–phalloidin (1:100; Invitrogen) or rhodamine–phalloidin (1:100; Invitrogen) to stain nuclei and F-actin, respectively. Tissues were then washed again in PBST, preserved in Gel/Mount aqueous mounting medium (Sigma-Aldrich), and coverslipped.

Images of single optical sections were collected on a laser-scanning confocal microscope (Radiance 2100; Bio-Rad Laboratories) mounted on a TE2000-U microscope (Nikon) using a 100×/1.4 NA oil objective lens (zoom 1 or 3) at RT. LaserSharp 2000 software (Bio-Rad Laboratories) was used during image collection. The gain and laser power were adjusted to stay within the fluorescent detector's linear range, and identical settings of the fluorescent imaging system were used to collect images of each set of stained sections from *Tmod1$^{+/+Tg+}$* and *Tmod1$^{-/-Tg+}$* animals. The ratios of M/Z or Z/P fluorescence were computed in ImageJ (National Institutes of Health) by placing a rectangular bounding box around three to five consecutive sarcomeres in a myofibril to generate a line scan, performing background correction using an adjacent myofibril-free region, and then integrating the areas under the fluorescence peaks corresponding to either the M line, Z line, or thin filament pointed ends. Fluorescence ratios were calculated from the grayscale single-channel TIFF images. To avoid error introduced by the nonlinearity of the fluorescence detector when collecting subthreshold or oversaturated signals, any myofibrils containing over- or underexposed pixels were excluded from the ratiometric analysis. Images were processed with Photoshop (Adobe), and image figures were constructed in Illustrator (Adobe).

Muscle sample preparation and Western blotting
For muscle fractionation experiments, TA muscles were dissected in ice-cold relaxing buffer, relaxed for 24 h at 4°C, and homogenized with a Tissumizer (Teledyne Tekmar) in 10 vol of ice-cold rigor buffer (100 mM KCl, 2 mM MgCl$_2$, 10 mM K$_3$PO$_4$, 1 mM EDTA, and 1 mM DTT, pH 7.0) supplemented with protease inhibitor cocktail (1:1,000; Sigma-Aldrich),

as previously described (Knight and Trinick, 1982; Fowler et al., 1993). The homogenate was centrifuged at 1,500 g for 5 min at 4°C, producing a low-speed pellet rich in myofibrils. After washing the low-speed pellet four times in rigor buffer, the low-speed supernatant was centrifuged at 15,000 g for 15 min at 4°C, producing a medium-speed pellet rich in organelles, membranes, and other extrasarcomeric structures. The resulting medium-speed supernatant was then centrifuged at 150,000 g for 15 min at 4°C, producing a high-speed pellet rich in microsomes and macromolecular complexes and a high-speed supernatant containing cytosol. Pellets were solubilized by sonication in 2× SDS sample buffer and by boiling for 5 min. Total homogenate and cytosol were solubilized by vortexing in 2× SDS sample buffer and by boiling for 5 min. For sample preparation without fractionation, EDL muscles were dissected and extracted by homogenization in 4 vol (volume/wet weight) of 9.2 M urea and solubilized in 1/5 vol of 5× SDS sample buffer and by boiling for 5 min. Human erythrocyte Mg^{2+} ghosts (Fowler and Bennett, 1984) and human umbilical vein endothelial cells (hUVECs) were solubilized by vortexing in 2× SDS sample buffer and by boiling for 5 min.

Proteins were separated via SDS-PAGE on 14% minigels and transferred to nitrocellulose in transfer buffer with 20% methanol at 4°C. For β2-spectrin, RyR1, and dystrophin blots, 8% minigels, 4–10% linear gradient minigels, and 4–15% linear gradient minigels were used, respectively, and proteins were transferred without methanol in 0.01% SDS (Nowak et al., 2009). For muscle fractionation, co-IP, and GST pull-down experiments, 4–20% linear gradient minigels were used. Blots were stained with 0.2% Ponceau S in 3% TCA to verify protein transfer, incubated in Blitz buffer (4% BSA, 10 mM $NaHPO_4$, pH 7.4, 150 mM NaCl, 1 mM EDTA, and 0.2% Triton X-100) for at least 2 h at RT, and then incubated in primary antibodies diluted in Blitz overnight at 4°C. After washing in PBST, blots were incubated in either HRP-conjugated Protein A (1:10,000; Sigma-Aldrich) or HRP-conjugated secondary antibodies diluted in Blitz + 2% donkey serum for 1–2 h at RT. After washing again in PBST, protein bands were detected using ECL. Blots were exposed for a series of times (1 s–5 min), followed by scanning, densitometry, and quantification using ImageJ. Only blots with intermediate exposures on the linear region of the signal intensity versus the exposure time curve were used thereafter. When appropriate, blots were controlled for loading by stripping and reprobing for total actin, using the same detection procedure. For muscle fractionation experiments, distributions were computed by expressing the intensities of the 1,500-g pellet, 15,000-g pellet, 150,000-g pellet, and cytosol bands as percentages of the sum of the intensities of all four bands.

co-IP

Mouse skeletal muscles were dissected in ice-cold PBS, homogenized with a Tissumizer in 10 vol of ice-cold RIPA buffer (150 mM NaCl, 1% NP-40, 0.5% sodium deoxycholate, 0.1% SDS, and 50 mM Tris-HCl, pH 8.0) supplemented with protease inhibitor cocktail (1:1,000), and clarified by 5 min of centrifugation at 1,500 g to remove myofibrils. The resulting SR-enriched extract was divided into 1-ml aliquots, to which one of the following was added: 2 µg rabbit polyclonal anti-sAnk1.5 (ARP42566_T100), 2 µg rabbit polyclonal anti–human Tmod1 (R1749), 5 µl rabbit polyclonal antiserum to human Tmod3 (R5168bl3c), 2 µg of preimmune control IgG, or 5 µl of preimmune control serum. Antibody-bound protein complexes were absorbed to 100 µl µMACS Protein A–conjugated super-paramagnetic MicroBeads (Miltenyi Biotec) and incubated for 30 min on ice, followed by passage through a µColumn (Miltenyi Biotec) using a µMACS magnetic separator (Miltenyi Biotec). Beads were washed with RIPA buffer and eluted with 100 µl of 1× SDS sample buffer according to the manufacturer's instructions. The input extract (diluted in 2× SDS sample buffer) and eluted immunoprecipitates were then subjected to SDS-PAGE and Western blotting, as described in the previous section.

GST pull-down assay

An excess (20 µl) of ProCatch glutathione resin (Miltenyi Biotec) was prewashed in binding buffer (20 mM Hepes, 60 mM NaCl, 0.5 mM EDTA, 1 mM NaN_3, and 0.1% Tween 20, pH 7.3), and 3 µg of either GST or GST-sAnk1.5 (a gift from M.A. Ackermann and R.J. Bloch, University of Maryland School of Medicine, Baltimore, MD; Borzok et al., 2007) was loaded onto the resin by incubation for 1 h at 4°C. The beads were then washed three times by centrifugation at 1,000 g for 5 min, decanting the resulting supernatant, and resuspension in 1 ml of fresh binding buffer. Next, 3 µg of purified recombinant human Tmod1 or Tmod3 (Yamashiro et al., 2010) was added for a final concentration of 3 µg/ml Tmod and incubated for 1 h at 4°C. The beads were centrifuged

at 1,000 g for 5 min, and the resulting supernatant (unbound fraction) was mixed with an equal volume of 2× SDS sample buffer. The beads were then washed three times, and the resulting pellet (bound fraction) was solubilized in an equal volume of 2× SDS sample buffer and clarified by centrifugation at 1,000 g for 5 min. Protein samples were then subjected to SDS-PAGE and either Coomassie blue staining or Western blotting, as described in the Muscle sample preparation and Western blotting section.

TEM

Mice were perfusion fixed in 4% PFA + 1.5% glutaraldehyde in 0.1 M cacodylate buffer on ice followed by dissection of soleus and EDL muscles and incubation for several hours in the same fixative. Fixation was continued overnight in 2.5% glutaraldehyde in 0.1 M cacodylate buffer, and tissues were washed in cacodylate buffer, fixed further in 1% OsO_4 in 0.1 M sodium cacodylate buffer for 2 h, again washed in cacodylate buffer, and then dehydrated in graded ethanols followed by propylene oxide and embedded in EMbed 812/Araldite (Electron Microscopy Sciences). Thick sections (1–2 µm) were cut, mounted on glass slides, and stained in toluidine blue for assessment of tissue structure and preservation on a light microscope. Subsequently, 60-nm thin sections were cut, mounted on copper slot grids coated with parlodion, and stained with uranyl acetate and lead citrate for examination on a transmission electron microscope (Philips CM100; FEI) at 80 kV. Images were collected using a charge-coupled device camera (Megaview III; Olympus).

Ca^{2+} release assay

TA muscles were dissected in PBS, and tendons and connective tissue were carefully removed. Muscles were rinsed thoroughly in PBS, and extracellular collagen was digested by gently agitating muscles in 5 vol of 1 mg/ml collagenase in Eagle's minimal essential medium for 2 h at 37°C. Muscle fibers were then dissociated by repeated pipette aspiration. The fiber suspension was added to a solution of ACh (Sigma-Aldrich) in minimal essential medium, which was serially diluted from 0.005 M to 5×10^{-12} M on a 96-well plate. ACh-induced Ca^{2+} flux from the SR was measured using a Fluo-4 Direct assay kit (Invitrogen) according to the manufacturer's instructions. A plate reader quantified the results of the assay at excitation and emission wavelengths of 494 and 516 nm, respectively. The increase in Ca^{2+} flux from the baseline was normalized to baseline ($\Delta Ca/Ca^0$) and plotted as a function of ACh concentration.

Statistics

A reanalysis of previously published data (Gokhin et al., 2010) revealed that the intraanimal muscle functional variability is as large as the interanimal variability. Thus, muscles from hindlimbs of the same animal were treated as independent samples. The normal distribution of data was evaluated using the Shapiro-Wilk test. Where appropriate, differences between genotype-dependent parameters were detected using the Student's t test. Data are presented as mean ± SD, and statistical significance was defined as $P < 0.05$. Statistical analysis was performed in Excel (Microsoft).

Online supplemental material

Fig. S1 demonstrates the specificities of our actin isoform–specific antibodies. Fig. S2 depicts the Z line–flanking localization of Tmod4. Fig. S3 shows that the deletion of Tmod1 does not alter the levels of extrasarcomeric cytoskeletal proteins. Fig. S4 shows that the deletion of Tmod1 does not alter the localization of ankyrin-B or obscurin. Fig. S5 shows negative controls for co-IP experiments showing that the deletion of Tmod1 disrupts the Tmod3–γ_{cyto}-actin–sAnk1.5 complex. Online supplemental material is available at http://www.jcb.org/cgi/content/full/jcb.201011128/DC1.

References

Allen, P.G., C.B. Shuster, J. Käs, C. Chaponnier, P.A. Janmey, and I.M. Herman. 1996. Phalloidin binding and rheological differences among actin isoforms. *Biochemistry*. 35:14062–14069. doi:10.1021/bi961326g

Almenar-Queralt, A., A. Lee, C.A. Conley, L. Ribas de Pouplana, and V.M. Fowler. 1999. Identification of a novel tropomodulin isoform, skeletal tropomodulin, that caps actin filament pointed ends in fast skeletal muscle. *J. Biol. Chem.* 274:28466–28475. doi:10.1074/jbc.274.40.28466

Bagnato, P., V. Barone, E. Giacomello, D. Rossi, and V. Sorrentino. 2003. Binding of an ankyrin-1 isoform to obscurin suggests a molecular link between the sarcoplasmic reticulum and myofibrils in striated muscles. *J. Cell Biol.* 160:245–253. doi:10.1083/jcb.200208109

Bang, M.L., C. Gregorio, and S. Labeit. 2002. Molecular dissection of the interaction of desmin with the C-terminal region of nebulin. *J. Struct. Biol.* 137:119–127. doi:10.1006/jsbi.2002.4457

Belyantseva, I.A., B.J. Perrin, K.J. Sonnemann, M. Zhu, R. Stepanyan, J. McGee, G.I. Frolenkov, E.J. Walsh, K.H. Friderici, T.B. Friedman, and J.M. Ervasti. 2009. Gamma-actin is required for cytoskeletal maintenance but not development. *Proc. Natl. Acad. Sci. USA*. 106:9703–9708. doi:10.1073/pnas.0900221106

Bennett, V., and J. Healy. 2008. Being there: cellular targeting of voltage-gated sodium channels in the heart. *J. Cell Biol.* 180:13–15. doi:10.1083/jcb.200712098

Borzok, M.A., D.H. Catino, J.D. Nicholson, A. Kontrogianni-Konstantopoulos, and R.J. Bloch. 2007. Mapping the binding site on small ankyrin 1 for obscurin. *J. Biol. Chem.* 282:32384–32396. doi:10.1074/jbc.M704089200

Chu, X., J. Chen, M.C. Reedy, C. Vera, K.L. Sung, and L.A. Sung. 2003. E-Tmod capping of actin filaments at the slow-growing end is required to establish mouse embryonic circulation. *Am. J. Physiol. Heart Circ. Physiol.* 284:H1827–H1838.

Conley, C.A., K.L. Fritz-Six, A. Almenar-Queralt, and V.M. Fowler. 2001. Leiomodins: larger members of the tropomodulin (Tmod) gene family. *Genomics*. 73:127–139. doi:10.1006/geno.2000.6501

Conover, G.M., S.N. Henderson, and C.C. Gregorio. 2009. A myopathy-linked desmin mutation perturbs striated muscle actin filament architecture. *Mol. Biol. Cell*. 20:834–845. doi:10.1091/mbc.E08-07-0753

Cox, P.R., and H.Y. Zoghbi. 2000. Sequencing, expression analysis, and mapping of three unique human tropomodulin genes and their mouse orthologs. *Genomics*. 63:97–107. doi:10.1006/geno.1999.6061

Craig, S.W., and J.V. Pardo. 1983. Gamma actin, spectrin, and intermediate filament proteins colocalize with vinculin at costameres, myofibril-to-sarcolemma attachment sites. *Cell Motil.* 3:449–462. doi:10.1002/cm.970030513

Cunha, S.R., and P.J. Mohler. 2009. Ankyrin protein networks in membrane formation and stabilization. *J. Cell. Mol. Med.* 13:4364–4376. doi:10.1111/j.1582-4934.2009.00943.x

Fischer, R.S., K.L. Fritz-Six, and V.M. Fowler. 2003. Pointed-end capping by tropomodulin3 negatively regulates endothelial cell motility. *J. Cell Biol.* 161:371–380. doi:10.1083/jcb.200209057

Fowler, V.M. 1987. Identification and purification of a novel Mr 43,000 tropomyosin-binding protein from human erythrocyte membranes. *J. Biol. Chem.* 262:12792–12800.

Fowler, V.M. 1990. Tropomodulin: a cytoskeletal protein that binds to the end of erythrocyte tropomyosin and inhibits tropomyosin binding to actin. *J. Cell Biol.* 111:471–481. doi:10.1083/jcb.111.2.471

Fowler, V.M., and V. Bennett. 1984. Tropomyosin: a new component of the erythrocyte membrane skeleton. *Prog. Clin. Biol. Res.* 159:57–71.

Fowler, V.M., M.A. Sussmann, P.G. Miller, B.E. Flucher, and M.P. Daniels. 1993. Tropomodulin is associated with the free (pointed) ends of the thin filaments in rat skeletal muscle. *J. Cell Biol.* 120:411–420. doi:10.1083/jcb.120.2.411

Fritz-Six, K.L., P.R. Cox, R.S. Fischer, B. Xu, C.C. Gregorio, H.Y. Zoghbi, and V.M. Fowler. 2003. Aberrant myofibril assembly in tropomodulin1 null mice leads to aborted heart development and embryonic lethality. *J. Cell Biol.* 163:1033–1044. doi:10.1083/jcb.200308164

Fukuzawa, A., S. Lange, M. Holt, A. Vihola, V. Carmignac, A. Ferreiro, B. Udd, and M. Gautel. 2008. Interactions with titin and myomesin target obscurin and obscurin-like 1 to the M-band: implications for hereditary myopathies. *J. Cell Sci.* 121:1841–1851. doi:10.1242/jcs.028019

Gallagher, P.G., and B.G. Forget. 1998. An alternate promoter directs expression of a truncated, muscle-specific isoform of the human ankyrin 1 gene. *J. Biol. Chem.* 273:1339–1348. doi:10.1074/jbc.273.3.1339

Gallagher, P.G., W.T. Tse, A.L. Scarpa, S.E. Lux, and B.G. Forget. 1997. Structure and organization of the human ankyrin-1 gene. Basis for complexity of pre-mRNA processing. *J. Biol. Chem.* 272:19220–19228. doi:10.1074/jbc.272.31.19220

Galustian, C., J. Dye, L. Leach, P. Clark, and J.A. Firth. 1995. Actin cytoskeletal isoforms in human endothelial cells in vitro: alteration with cell passage. *In Vitro Cell. Dev. Biol. Anim.* 31:796–802. doi:10.1007/BF02634122

Gokhin, D.S., R.A. Lewis, C.R. McKeown, R.B. Nowak, N.E. Kim, R.S. Littlefield, R.L. Lieber, and V.M. Fowler. 2010. Tropomodulin isoforms regulate thin filament pointed-end capping and skeletal muscle physiology. *J. Cell Biol.* 189:95–109. doi:10.1083/jcb.201001125

Gregorio, C.C., A. Weber, M. Bondad, C.R. Pennise, and V.M. Fowler. 1995. Requirement of pointed-end capping by tropomodulin to maintain actin filament length in embryonic chick cardiac myocytes. *Nature*. 377:83–86. doi:10.1038/377083a0

Hanft, L.M., I.N. Rybakova, J.R. Patel, J.A. Rafael-Fortney, and J.M. Ervasti. 2006. Cytoplasmic gamma-actin contributes to a compensatory remodeling response in dystrophin-deficient muscle. *Proc. Natl. Acad. Sci. USA*. 103:5385–5390. doi:10.1073/pnas.0600980103

Hanft, L.M., D.J. Bogan, U. Mayer, S.J. Kaufman, J.N. Kornegay, and J.M. Ervasti. 2007. Cytoplasmic gamma-actin expression in diverse animal models of muscular dystrophy. *Neuromuscul. Disord.* 17:569–574. doi:10.1016/j.nmd.2007.03.004

Jaeger, M.A., K.J. Sonnemann, D.P. Fitzsimons, K.W. Prins, and J.M. Ervasti. 2009. Context-dependent functional substitution of alpha-skeletal actin by gamma-cytoplasmic actin. *FASEB J.* 23:2205–2214. doi:10.1096/fj.09-129783

Kee, A.J., G. Schevzov, V. Nair-Shalliker, C.S. Robinson, B. Vrhovski, M. Ghoddusi, M.R. Qiu, J.J. Lin, R. Weinberger, P.W. Gunning, and E.C. Hardeman. 2004. Sorting of a nonmuscle tropomyosin to a novel cytoskeletal compartment in skeletal muscle results in muscular dystrophy. *J. Cell Biol.* 166:685–696. doi:10.1083/jcb.200406181

Knight, P.J., and J.A. Trinick. 1982. Preparation of myofibrils. *Methods Enzymol.* 85:9–12. doi:10.1016/0076-6879(82)85004-0

Kontrogianni-Konstantopoulos, A., E.M. Jones, D.B. Van Rossum, and R.J. Bloch. 2003. Obscurin is a ligand for small ankyrin 1 in skeletal muscle. *Mol. Biol. Cell*. 14:1138–1148. doi:10.1091/mbc.E02-07-0411

Lange, S., K. Ouyang, G. Meyer, L. Cui, H. Cheng, R.L. Lieber, and J. Chen. 2009. Obscurin determines the architecture of the longitudinal sarcoplasmic reticulum. *J. Cell Sci.* 122:2640–2650. doi:10.1242/jcs.046193

Littlefield, R.S., and V.M. Fowler. 2008. Thin filament length regulation in striated muscle sarcomeres: pointed-end dynamics go beyond a nebulin ruler. *Semin. Cell Dev. Biol.* 19:511–519. doi:10.1016/j.semcdb.2008.08.009

Littlefield, R., A. Almenar-Queralt, and V.M. Fowler. 2001. Actin dynamics at pointed ends regulates thin filament length in striated muscle. *Nat. Cell Biol.* 3:544–551. doi:10.1038/35078517

McKeown, C.R., R.B. Nowak, J. Moyer, M.A. Sussman, and V.M. Fowler. 2008. Tropomodulin1 is required in the heart but not the yolk sac for mouse embryonic development. *Circ. Res.* 103:1241–1248. doi:10.1161/CIRCRESAHA.108.178749

Meyer, G.A., B. Kiss, S.R. Ward, D.L. Morgan, M.S. Kellermayer, and R.L. Lieber. 2010. Theoretical predictions of the effects of force transmission by desmin on intersarcomere dynamics. *Biophys. J.* 98:258–266. doi:10.1016/j.bpj.2009.10.014

Miller, J.B. 1991. Myoblasts, myosins, MyoDs, and the diversification of muscle fibers. *Neuromuscul. Disord.* 1:7–17. doi:10.1016/0960-8966(91)90038-T

Milner, D.J., G. Weitzer, D. Tran, A. Bradley, and Y. Capetanaki. 1996. Disruption of muscle architecture and myocardial degeneration in mice lacking desmin. *J. Cell Biol.* 134:1255–1270. doi:10.1083/jcb.134.5.1255

Mohler, P.J., J.Q. Davis, and V. Bennett. 2005. Ankyrin-B coordinates the Na/K ATPase, Na/Ca exchanger, and InsP3 receptor in a cardiac T-tubule/SR microdomain. *PLoS Biol.* 3:e423. doi:10.1371/journal.pbio.0030423

Monti, R.J., R.R. Roy, J.A. Hodgson, and V.R. Edgerton. 1999. Transmission of forces within mammalian skeletal muscles. *J. Biomech.* 32:371–380. doi:10.1016/S0021-9290(98)00189-4

Moyer, J.D., R.B. Nowak, N.E. Kim, S.K. Larkin, L.L. Peters, J. Hartwig, F.A. Kuypers, and V.M. Fowler. 2010. Tropomodulin 1-null mice have a mild spherocytic elliptocytosis with appearance of tropomodulin 3 in red blood cells and disruption of the membrane skeleton. *Blood*. 116:2590–2599. doi:10.1182/blood-2010-02-268458

Nelson, W.J., and E. Lazarides. 1983. Expression of the beta subunit of spectrin in nonerythroid cells. *Proc. Natl. Acad. Sci. USA*. 80:363–367. doi:10.1073/pnas.80.2.363

Nowak, R.B., R.S. Fischer, R.K. Zoltoski, J.R. Kuszak, and V.M. Fowler. 2009. Tropomodulin1 is required for membrane skeleton organization and hexagonal geometry of fiber cells in the mouse lens. *J. Cell Biol.* 186:915–928. doi:10.1083/jcb.200905065

Otey, C.A., M.H. Kalnoski, and J.C. Bulinski. 1988. Immunolocalization of muscle and nonmuscle isoforms of actin in myogenic cells and adult skeletal muscle. *Cell Motil. Cytoskeleton*. 9:337–348. doi:10.1002/cm.970090406

Otterbein, L.R., P. Graceffa, and R. Dominguez. 2001. The crystal structure of uncomplexed actin in the ADP state. *Science*. 293:708–711. doi:10.1126/science.1059700

Pardo, J.V., M.F. Pittenger, and S.W. Craig. 1983. Subcellular sorting of isoactins: selective association of gamma actin with skeletal muscle mitochondria. *Cell*. 32:1093–1103. doi:10.1016/0092-8674(83)90293-3

Porter, G.A., G.M. Dmytrenko, J.C. Winkelmann, and R.J. Bloch. 1992. Dystrophin colocalizes with β-spectrin in distinct subsarcolemmal domains in mammalian skeletal muscle. *J. Cell Biol.* 117:997–1005. doi:10.1083/jcb.117.5.997

Porter, G.A., M.G. Scher, W.G. Resneck, N.C. Porter, V.M. Fowler, and R.J. Bloch. 1997. Two populations of beta-spectrin in rat skeletal muscle. *Cell Motil. Cytoskeleton*. 37:7–19. doi:10.1002/(SICI)1097-0169(1997)37:1<7::AID-CM2>3.0.CO;2-7

Porter, N.C., W.G. Resneck, A. O'Neill, D.B. Van Rossum, M.R. Stone, and R.J. Bloch. 2005. Association of small ankyrin 1 with the sarcoplasmic reticulum. *Mol. Membr. Biol.* 22:421–432. doi:10.1080/09687860500244262

Prins, K.W., D.A. Lowe, and J.M. Ervasti. 2008. Skeletal muscle-specific ablation of gamma(cyto)-actin does not exacerbate the mdx phenotype. *PLoS ONE*. 3:e2419. doi:10.1371/journal.pone.0002419

Renley, B.A., I.N. Rybakova, K.J. Amann, and J.M. Ervasti. 1998. Dystrophin binding to nonmuscle actin. *Cell Motil. Cytoskeleton*. 41:264–270. doi:10.1002/(SICI)1097-0169(1998)41:3<264::AID-CM7>3.0.CO;2-Z

Repasky, E.A., B.L. Granger, and E. Lazarides. 1982. Widespread occurrence of avian spectrin in nonerythroid cells. *Cell*. 29:821–833. doi:10.1016/0092-8674(82)90444-5

Rybakova, I.N., J.R. Patel, and J.M. Ervasti. 2000. The dystrophin complex forms a mechanically strong link between the sarcolemma and costameric actin. *J. Cell Biol.* 150:1209–1214. doi:10.1083/jcb.150.5.1209

Shah, S.B., F.C. Su, K. Jordan, D.J. Milner, J. Fridén, Y. Capetanaki, and R.L. Lieber. 2002. Evidence for increased myofibrillar mobility in desmin-null mouse skeletal muscle. *J. Exp. Biol.* 205:321–325.

Shah, S.B., J. Davis, N. Weisleder, I. Kostavassili, A.D. McCulloch, E. Ralston, Y. Capetanaki, and R.L. Lieber. 2004. Structural and functional roles of desmin in mouse skeletal muscle during passive deformation. *Biophys. J.* 86:2993–3008. doi:10.1016/S0006-3495(04)74349-0

Sonnemann, K.J., D.P. Fitzsimons, J.R. Patel, Y. Liu, M.F. Schneider, R.L. Moss, and J.M. Ervasti. 2006. Cytoplasmic gamma-actin is not required for skeletal muscle development but its absence leads to a progressive myopathy. *Dev. Cell*. 11:387–397. doi:10.1016/j.devcel.2006.07.001

Sung, L.A., V.M. Fowler, K. Lambert, M.A. Sussman, D. Karr, and S. Chien. 1992. Molecular cloning and characterization of human fetal liver tropomodulin. A tropomyosin-binding protein. *J. Biol. Chem.* 267:2616–2621.

Tonino, P., C.T. Pappas, B.D. Hudson, S. Labeit, C.C. Gregorio, and H. Granzier. 2010. Reduced myofibrillar connectivity and increased Z-disk width in nebulin-deficient skeletal muscle. *J. Cell Sci.* 123:384–391. doi:10.1242/jcs.042234

Vlahovich, N., G. Schevzov, V. Nair-Shaliker, B. Ilkovski, S.T. Artap, J.E. Joya, A.J. Kee, K.N. North, P.W. Gunning, and E.C. Hardeman. 2008. Tropomyosin 4 defines novel filaments in skeletal muscle associated with muscle remodelling/regeneration in normal and diseased muscle. *Cell Motil. Cytoskeleton*. 65:73–85. doi:10.1002/cm.20245

Vlahovich, N., A.J. Kee, C. Van der Poel, E. Kettle, D. Hernandez-Deviez, C. Lucas, G.S. Lynch, R.G. Parton, P.W. Gunning, and E.C. Hardeman. 2009. Cytoskeletal tropomyosin Tm5NM1 is required for normal excitation-contraction coupling in skeletal muscle. *Mol. Biol. Cell*. 20:400–409. doi:10.1091/mbc.E08-06-0616

Watakabe, A., R. Kobayashi, and D.M. Helfman. 1996. N-tropomodulin: a novel isoform of tropomodulin identified as the major binding protein to brain tropomyosin. *J. Cell Sci.* 109:2299–2310.

Weber, K.L., R.S. Fischer, and V.M. Fowler. 2007. Tmod3 regulates polarized epithelial cell morphology. *J. Cell Sci.* 120:3625–3632. doi:10.1242/jcs.011445

Williams, M.W., W.G. Resneck, T. Kaysser, J.A. Ursitti, C.S. Birkenmeier, J.E. Barker, and R.J. Bloch. 2001. Na,K-ATPase in skeletal muscle: two populations of beta-spectrin control localization in the sarcolemma but not partitioning between the sarcolemma and the transverse tubules. *J. Cell Sci.* 114:751–762.

Woo, M.K., A. Lee, R.S. Fischer, J. Moyer, and V.M. Fowler. 2000. The lens membrane skeleton contains structures preferentially enriched in spectrin-actin or tropomodulin-actin complexes. *Cell Motil. Cytoskeleton*. 46:257–268. doi:10.1002/1097-0169(200008)46:4<257::AID-CM3>3.0.CO;2-2

Yamashiro, S., K.D. Speicher, D.W. Speicher, and V.M. Fowler. 2010. Mammalian tropomodulins nucleate actin polymerization via their actin monomer binding and filament pointed end-capping activities. *J. Biol. Chem.* 285:33265–33280. doi:10.1074/jbc.M110.144873